Conceptual Design of Coaxial Injector for Laser Ignition Source

a project presented to

The Faculty of the Department of Aerospace Engineering

San José State University

in partial fulfillment of the requirements for the degree

Master of Science in Aerospace Engineering

by

Cristopher A. Barillas

May 2024

approved by

Dr. Periklis Papadopoulos

Faculty Advisor

ABSTRACT

Conceptual Design Coaxial Injector for Laser Ignition Source

Cristopher A. Barillas

The purpose of this paper is to design a coaxial injector and attach a laser ignition system to the injector manifold to deposit a kernel of ionized air that causes ignition of a LOX (Liquid Oxygen) and H2 (Hydrogen Gas) mixture. This paper will focus on the fluid mixture assuming the miniaturized laser has the needed energy to cause ignition at low temperatures.

Acknowledgments

I would like to thank my friends and family for pushing me this far in my education as well as my co-workers for igniting an interest in the topic and seeing the many accomplishments that can be achieved with such technologies.

Table of Contents

List of Figures

List of Tables

Nomenclature

Symbol	Definition	Units (SI)
A	Swirl Chamber Area	m^2
d_0	Diameter of Injector exit	m
D_s	Diameter of Swirl Chamber	m
K	K Constant	
ΔP_L	Pressure Drop Injector	Pa
θ_m	Spray Cone Angle	deg
ρ_L	Density	$\frac{kg}{m^3}$
μ_L^2	Dynamic Viscosity	Pa-s

1 Introduction, Literature Review and Methodology

1.1 Motivation

Current technology for the ignition of rockets by propellant engines is dependent on spark plug technology. This technology and design come with issues, such as oxygen supply, reusability, and high levels of electromagnetic interference (EMF) [1]. These issues are an engineering problem that has a possible solution with the incorporation of a laser ignition system. Specifically, the laser ablation [1] approach for ignition of mixtures can replace spark plug technology with none of the drawbacks. EMF can cause issues to other critical electronically dependent components. Oxygen supply is important as the operation of spark plugs requires a high level of oxygen. Reusability will also be achievable with the stem only needing power to start. Laser systems could be incorporated into existing systems [2] and reduce the needed redesign of critical components of current rocket engines. The laser ignition system is not limited to engine ignition applications, as it can also be integrated into other systems from the approach of a pulser laser power [3].

1.2 Literature Review

1.2.1 Laser Ablation Ignition Physics

The methodology on how to ignite bi-propellant fuel has already been tested and proven with the laser ablation method, [4] or direct laser ignition via non-resonant breakdown of the propellants [5] which will be explained in the next section. Laser ablation is the process where a high amount of concentrated energy from a laser hits a metal surface causing a reaction where in a very short time frame, the surface of the metal transitions from solid to plasma [3]. The process can be seen in Figure 1.1.

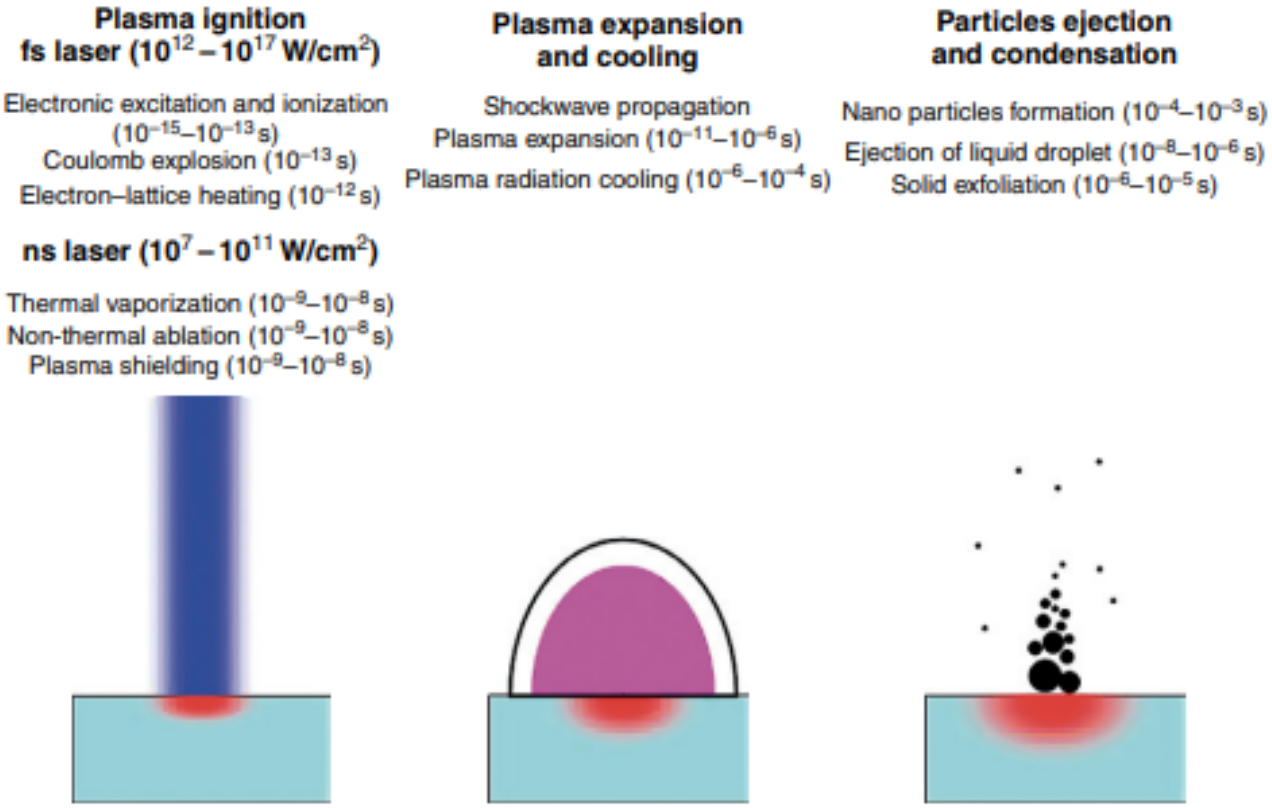

Figure 1.1 - Laser ablation process during each step and time frame during the process [3]

This plasma can reach 2000 to 3000 K (Kelvin) which is needed to ignite the fuel and an oxidizer mixture of Oxygen and kerosene, ethanol, or Hydrogen [1]. This plasma transfers the heat it generates to the ambient after hitting the target in an expansive plume as shown in Figure 1.2.

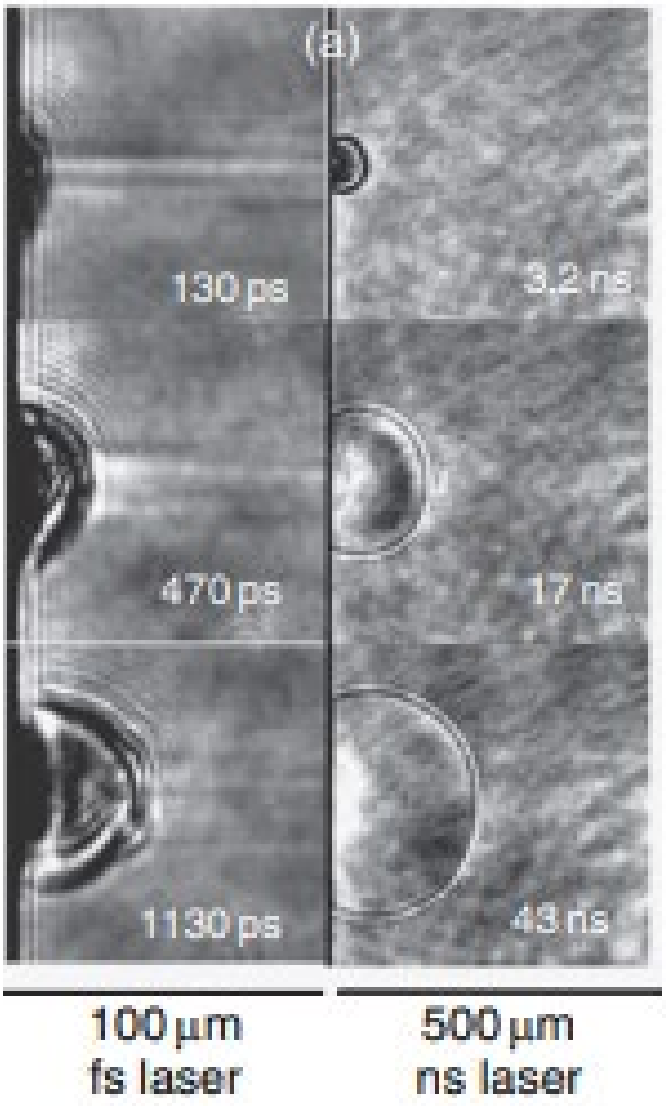

Figure 1.2 - Femto and nano second expansive plasma plume [3]

To replicate this, a Stainless-Steel Ball (SST) was used as the target to generate plasma. This is incorporated into a design that was proposed as a simplified model. The test that has been conducted uses oxygen and is being injected into a centrifugal chamber and supply holes. This is shown in Figure 1.3, which also includes the infrastructure needed to achieve ignition through a radiation source that will run through a fiber optic with the right intensity to achieve plasma production. The radiation source for the gases mentioned needs to have anywhere from 1050 nm to 1060 nm in wavelength. This plasma production will thus dissipate the heat and energy needed to ignite the fuel oxidizer mixture. Figure 1.4 shows the laser ignition happening due to laser ablation.

In the case of most laser sources an ND:YAG 1064 nm laser or HiPoLas ® laser is used with relative repeatability. As seen in Figure 1.5, a HiPoLas Laser system is used in the side of the thrust hitting the metal of the injector faceplate to cause ablative ignition.

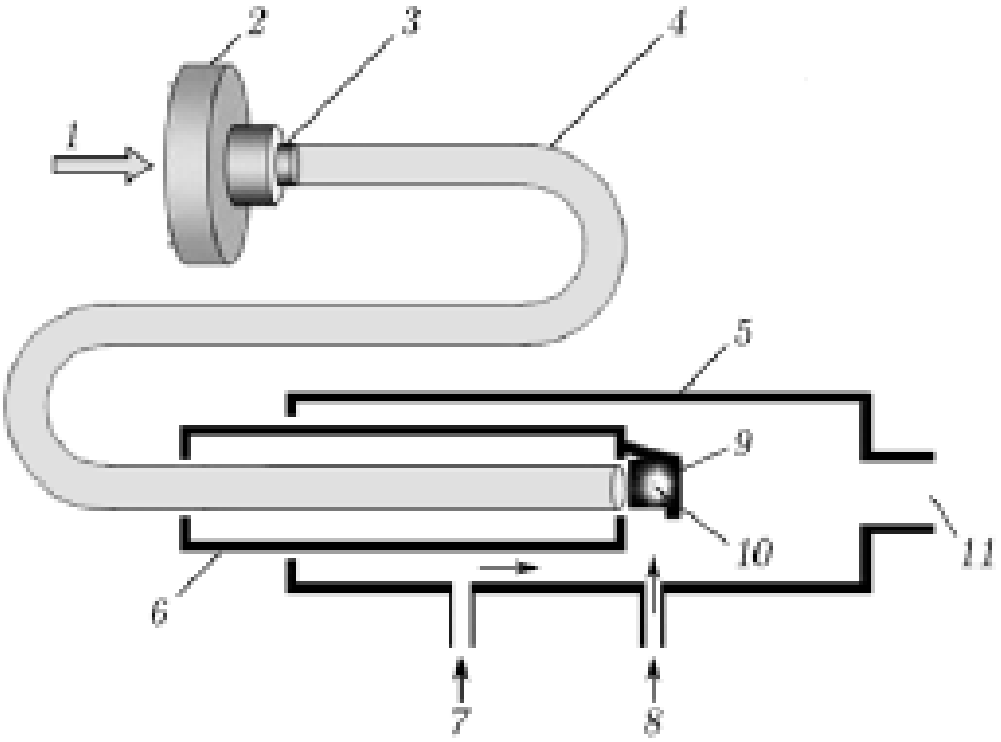

Figure 1.3 - Conceptual design for ignition of fuel through a laser system [1]

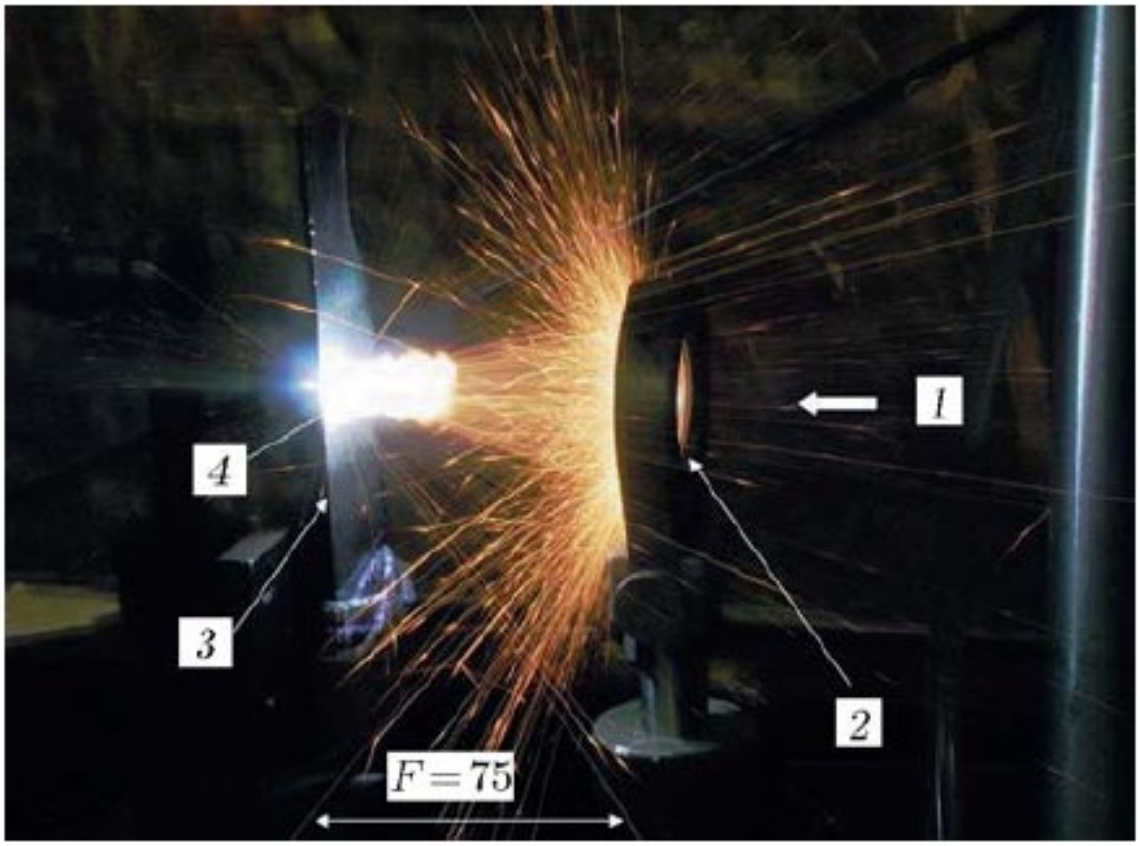

Figure 1.4 - Laser ablation ignition on steel surface [1]

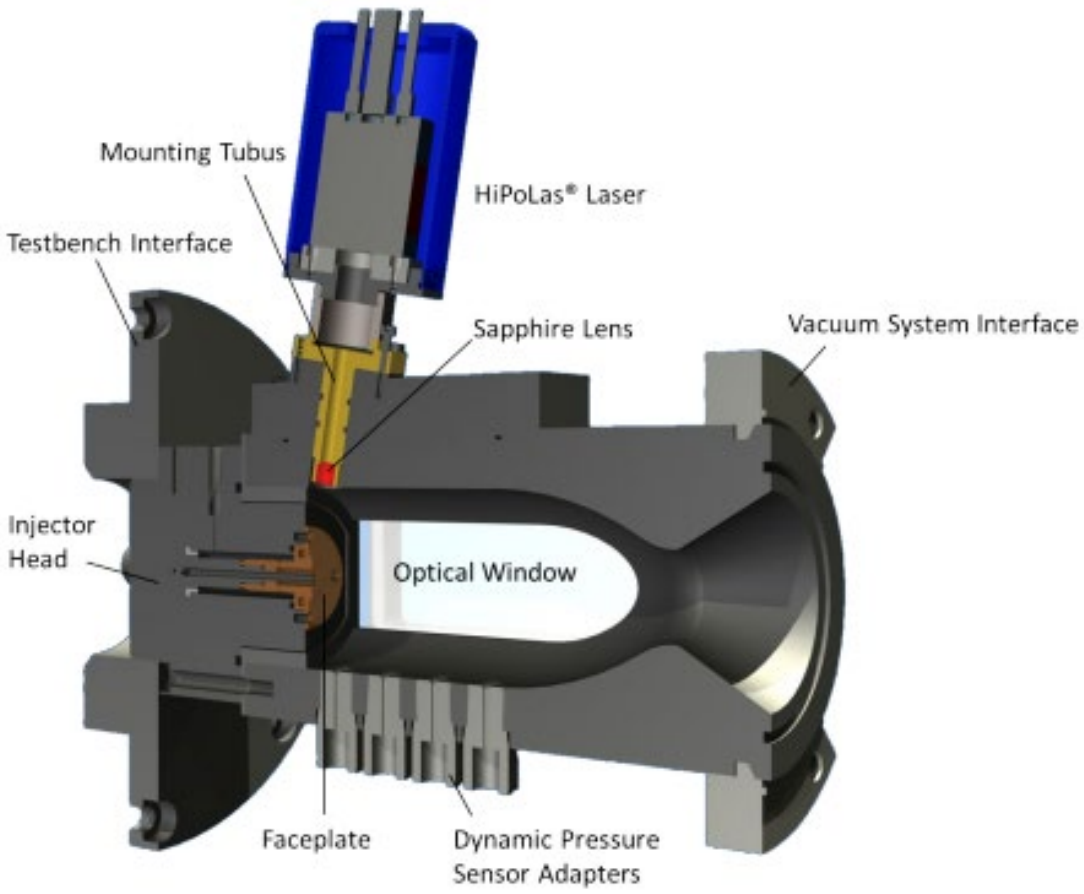

Figure 1.5 HiPoLas laser on the side of thruster [6]

Existing systems that have been tested for cryogenic and bi-propellant systems have shown the concept to work for single and multiple ignitions. One such system uses a pulsed laser system mounted directly to the combustion chamber with a lens to focus the beam [5]. This was used for ablative ignition and generation of plasma when it contacts the edge of the injector plate hole. This tested engine as shown in Figure 1.6, used LOX and hydrogen as well as LOX and Methane to show the ignition and reignition possibility with laser successfully. The laser needed to achieve ignition of the cryogenic gases mentioned had to have an intensity of $10^{11} W/cm^2$ and, achieve a temperature of plasma $10^5\ K$ to ignite the propellants.

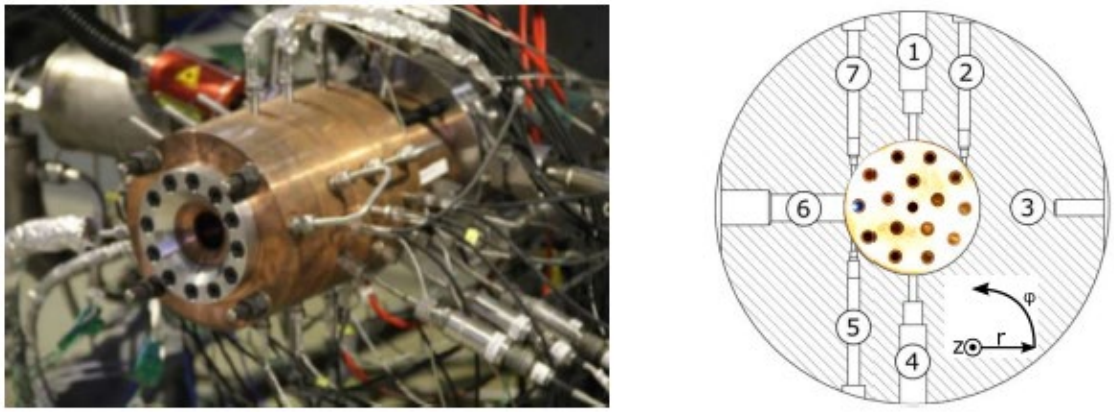

Figure 1.6 - DLR Institute of Space Propulsion, Germany laser ignition cryogenic engine [5]

Test runs to show the re-ignition using the laser system with a total of 1755 tests were performed and showed consistent results [5]. Figure 1.7 shows a test run conducted, which shows a combustion chamber pressure of 7 bar or about 101 psi for ignition to be consistently achieved. The project showed the application of a laser system and the reliability of being viable.

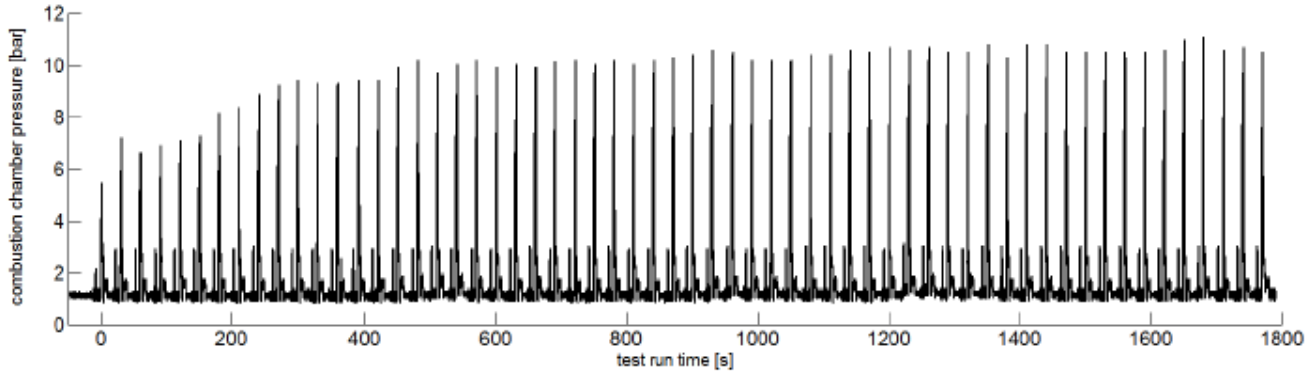

Figure 1.7 - Test run showing consistent re-ignition of DLR's Engine over time with 60 consecutive ignition runs [5]

1.2.2 Direct Laser Ignition

Direct laser ignition is a process where a laser is focused in air and ionizes the air to form a flame kernel of stored energy. This energy when in contact with a gas or liquid mixture can

transfer the energy to provide the necessary heat for ignition. As seen in Figure 1.8, a flame kernel for a laser ignition source is seen ionized in air compared to the left image of a normal car spark plug. The process uses pulse power to make the constant-volume flame kernel in which a maximum output energy of 16 mJ is possible in 4mJ pulses, with the four pulses having a width of 0.6 ns. Figure 1.9 shows the pulse energy laser in air being ionized.

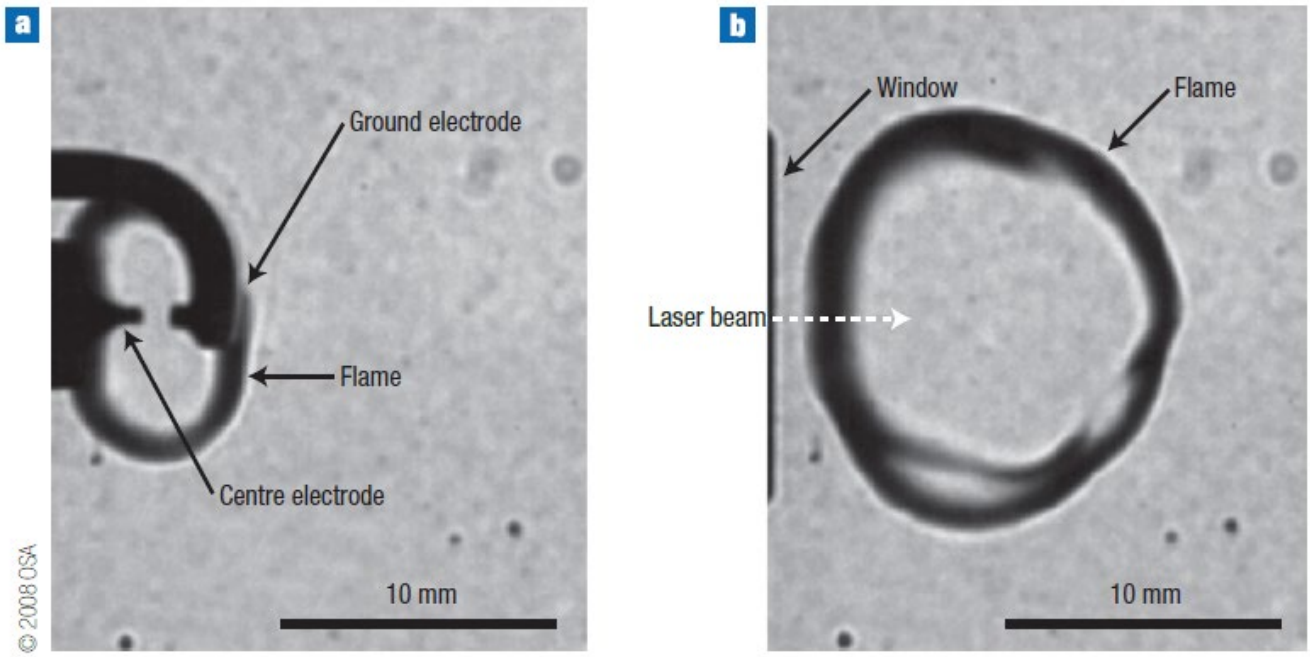

Figure 1.8 - Conventional spark plug flame kernal vs laser flame kernel [7]

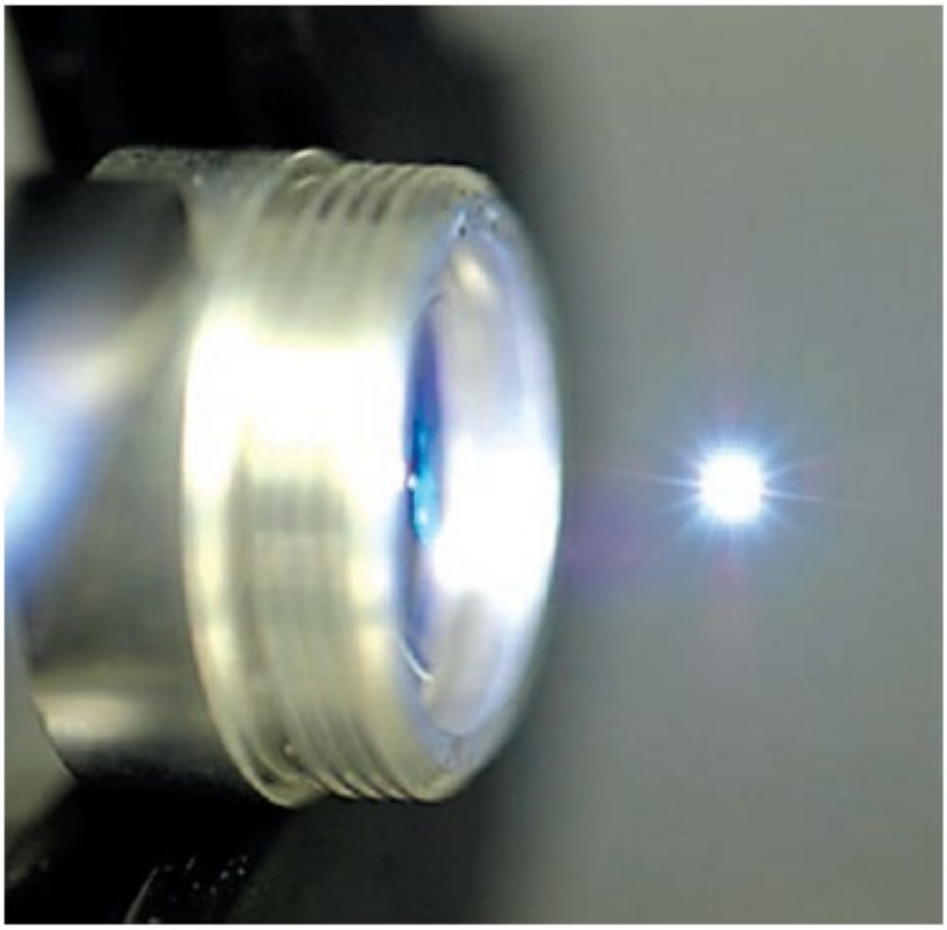

Figure 1.9 - Ionization of air by 2.7mJ laser [7]

Companies such as Toyota have put effort into minorizing the technology to allow for a more efficient and cost-effective alternative to conventional spark plugs in automotive combustion. As seen in Figure 1.10, a proposed conceptual schematic for a laser-ignited combustion engine is possible. It has also been used in the ignition of a Wankel Engine [4] and various fuel sources such as nitro and butane.

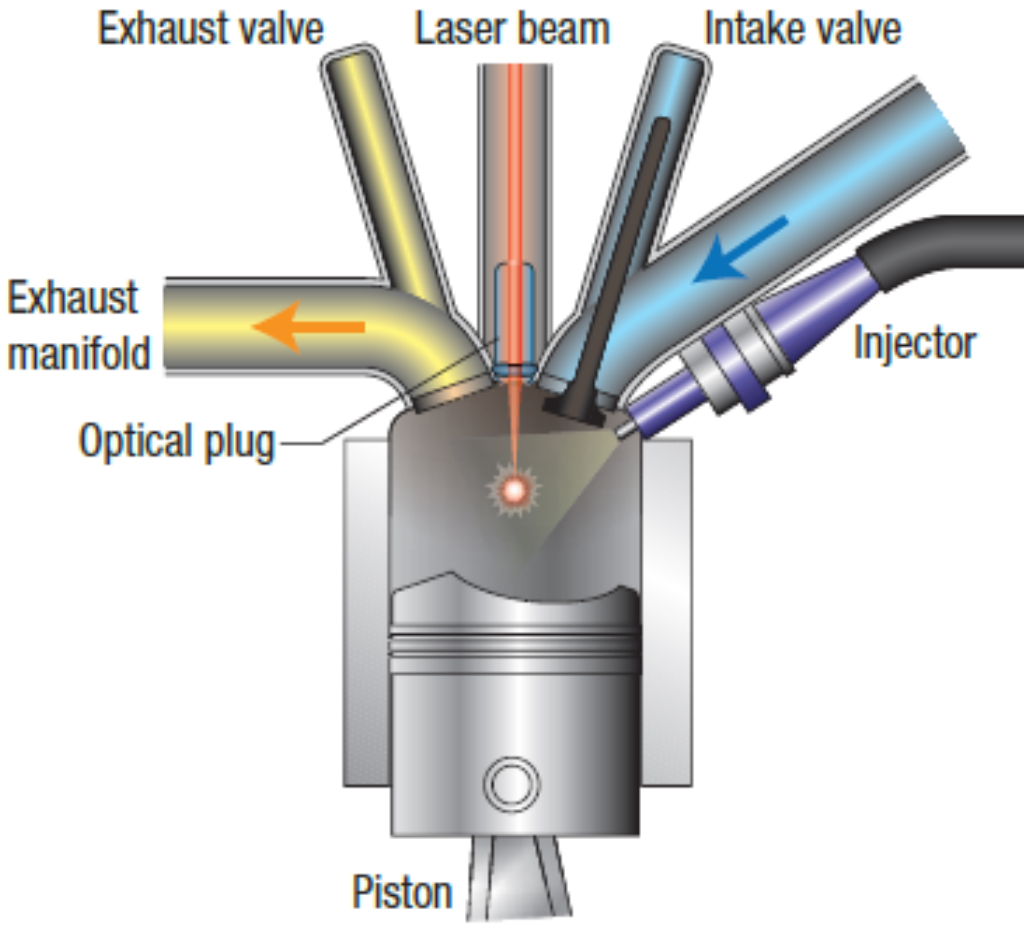

Figure 1.10 - Laser combustion engine schematic [7]

As this method of ignition is a point of deposited energy, an oblique detonation wave is a viable option for treating the combustion process. As shown in Figure 1.11, a wave of the conical wave can then match the geometry of the nozzle to get an efficient process. Numerically it has been used in a rotary engine using hydrogen combustion [8].

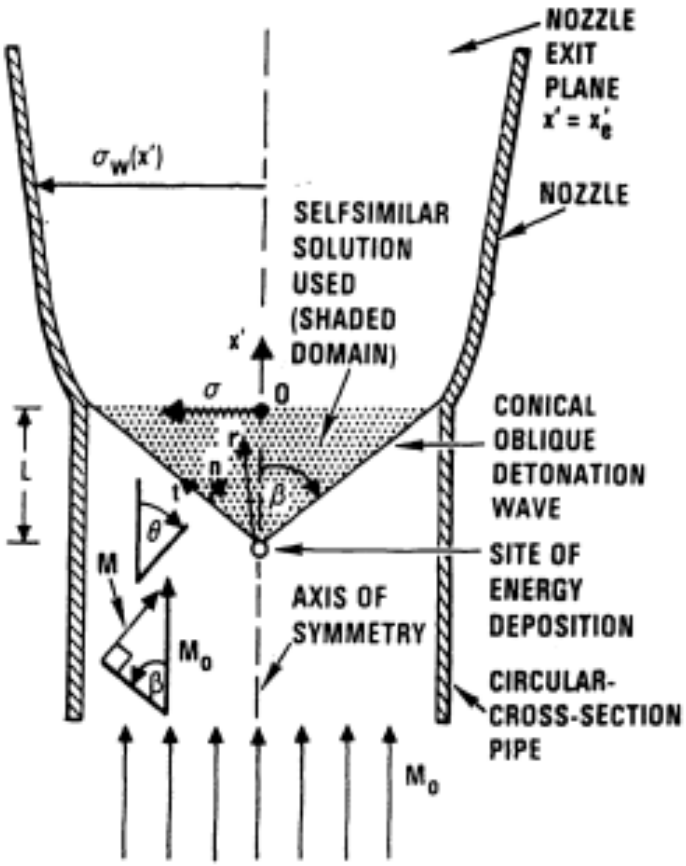

Figure 1.11 - Conceptual oblique detonation wave through direct laser ignition [9]

Other than the mentioned direct ignition source, other notable ways of achieving ignition through direct contact with fluids are photochemical, non-resonant, thermal, and resonant laser [10].

1.2.3 Rocket Injector Design

Rocket thrust engines need a method to atomize and send the fuel and oxidizer mixture into the combustion chamber. As such understanding and picking a manifold type that can integrate with a laser is important. Like Figure 1.7, the ignition occurs due to the laser creating plasma at the injector when it meets the edge of the face. This shoots plasma and metallic pieces that transfer heat to the atomized fuel mixture and cause ignition. Most common manifolds are like that of Figure 1.10, where fuel and oxidizer are injected through a feed system.

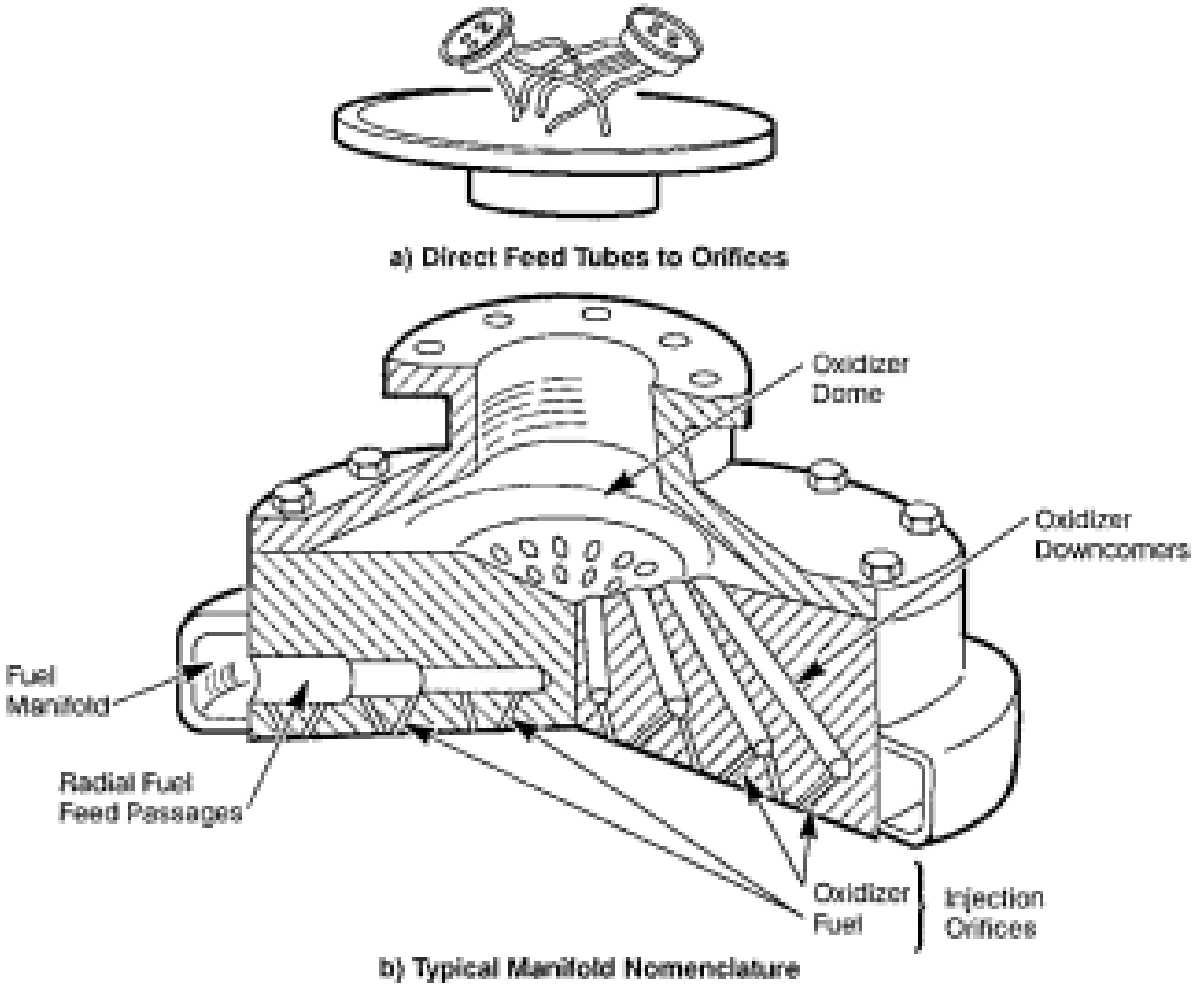

Figure 1.12 - Injector manifold and structure [11]

Though the importance of laser ignition, moving away from the conventional oxidizer fuel from above following a path much like the fuel source, and meeting the correct parameters for a safe and efficient injection is key. Table 1.1 shows the typical injector elements that are used. This is the main contributing factor that will be used in deciding the design of the system.

Table 1.1 - Comparison of typical injector elements for gas/liquid injection [11]

ELEMENT DESIGNATION	ELEMENT CONFIGURATION (FLOW DIRECTION)	ADVANTAGES	DISADVANTAGES	DESIGN CORRELATIONS*	ENGINE APPLICATION
UNLIKE TRIPLET (2 ON 1) ●○●	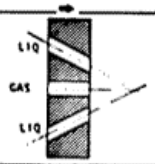	Excellent atomization Good overall mixing Resultant spray direction is axial	Wall compatibility is good only when fuel is used in outer orifices Sensitive to design tolerances Performance sensitive to continuous throttling	Mixing (ref. 12) Atomization (ref. 12)	None known
UNLIKE PENTAD (4 ON 1) ●○● ●	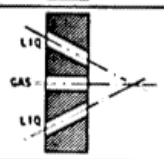	Excellent atomization Good overall mixing Applicable to extremely high or low mixture ratios or density ratios Well characterized	Difficult to manifold Wall compatibility problems Performance sensitive to throttling Tends to produce high heat flux to injector face	Mixing (ref. 12) Atomization (ref. 12)	None known
CONCENTRIC TUBE (WITH SWIRLER)	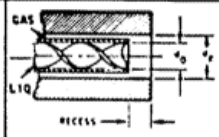	Excellent mixing and atomization Low pressure drop Proven dependability	Difficult to fabricate if annulus gap is very small (< 0.06 in.) Tends to become unstable when throttled	Generalized (ref. 13)	J-2, RL-10, M-1 Russians use this element extensively
CONCENTRIC TUBE (WITHOUT SWIRLER)	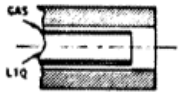	Very good wall compatibility Low pressure drop Excellent atomization	Same as above	Mixing (refs. 5 and 14) Atomization (refs. 5 and 14)	
LIKE DOUBLET (1 ON 1) ● OR ● ○ ○	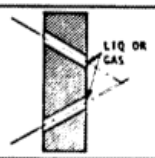	Easy to manifold Excellent for deliberate control of spray for wall temperature Good mixing Very stable element	Requires increased axial distances to mix the fuel and oxidizer Sensitive to design tolerances	None	None known

1.2.4 Coaxial Injectors

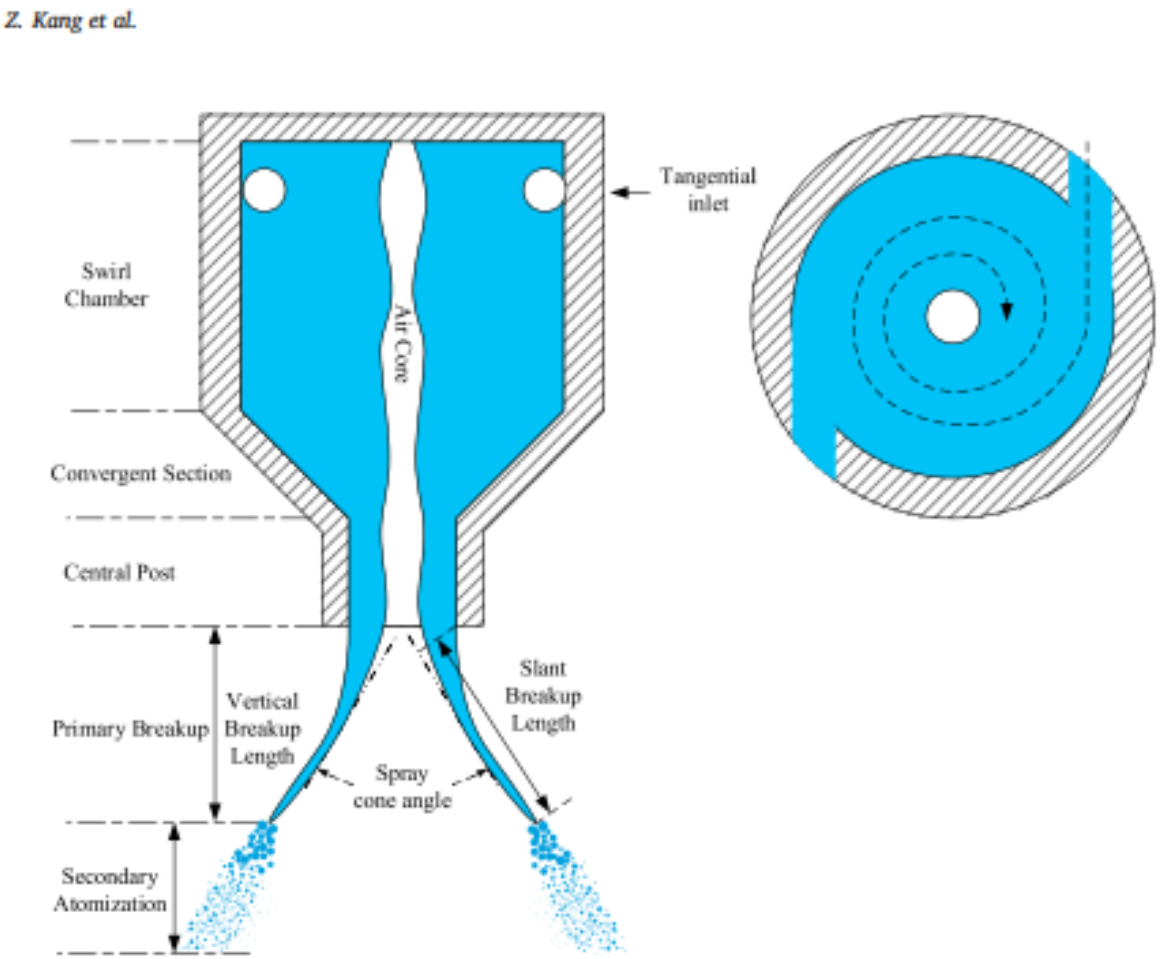

Figure 1.13 - Coaxial injector workings [12]

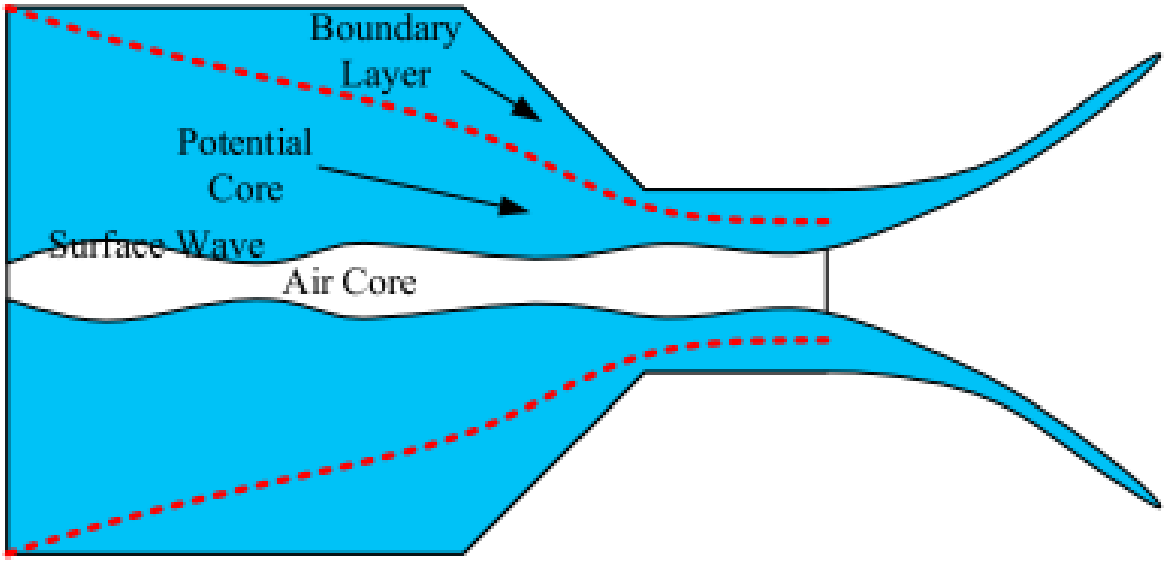

Figure 1.14 - Boundary layer formation in swirl injector [12]

Coaxial injectors work by having tangential holes in the structure that induce a tangential velocity into the injector. As seen in Figure 1.13, an air cone in the center is produced by the swirling of the fluid. This also creates a boundary layer along the edge of the swirler as seen in Figure 1.14. As the fluid converges into the central post a boundary and into the chamber, it will break up and then atomize. While the nature of these injectors is understood, the derived experimental data and equations have varied in different experiments. Equations such as for film, thickness, discharge coefficient, spray cone angle, and breakup length, change depending on the medium and injector type [12]. Table 1.2 shows the different equations that have been derived either theoretically or experimentally for spray cone angles. With all equations, the factor that contributed the most was found to be the K constant which is controlled by the geometrical variation [12] and inlet pressure.

Table 1.2 - Coaxial injector spray cone angle equations [12]

Equations of the spray cone angle.

Author	Equation	Type	Injector type
Rizk and Lefebvre [59]	$\cos\beta = \frac{C_d}{K_v(1-X)}$, $C_d = K_v\left[\frac{(1-X)^3}{1+X}\right]^{0.5}$	Theoretical	
	$\cos^2\beta = \frac{1-X}{1+X}$		
Rizk(Liu et al. [14])	$\cos\beta = \frac{C_d}{K_v(1-X)} = \frac{0.35K^{0.5}(D_s/D_0)^{0.25}}{K_v(1-X)}$	Theoretical	
	$K_v = 0.00367K^{0.29}\left(\frac{\Delta P_l \rho_l}{\mu_l}\right)^{0.2}$		
Liu [67]	$\cos\beta = 0.302(1+\tan\vartheta)^{0.414}\left(\frac{1}{A}\right)^{0.35} \times \left(\frac{L_0}{D_0}\right)^{0.043}\left(\frac{D_s}{D_0}\right)^{0.026} + 0.612$	Experimental	Converge-end
Giffen and Muraszew	$\sin\beta = \frac{\pi C_d}{2K(1+\sqrt{X})} = \frac{(\pi/2)(1-X)^{1.5}}{K(1+\sqrt{X})(1+X)^{0.5}}$	Theoretical	
(Santangelo [108], Couto et al. [63] and Jeng et al. [48])	$C_d = \left[\frac{(1-X)^3}{1+X}\right]^{0.5}$, $K^2 = \frac{\pi^2(1-X)^3}{32X^2}$		
Xue et al. [15]	$\sin\beta = \frac{\pi C_d \sin\vartheta}{2K(1+\sqrt{X})}\left(\frac{R_{sw}}{R_s}\right)$	Theoretical	
	$K^2 = \frac{\pi^2(1-X)^3}{32X^2}\left(\frac{R_{sw}}{R_s}\right)^2\sin^2\vartheta$		
	$R_{sw} = R_s - R_t$		
Giffen and Muraszew (Liu et al. [22])	$\tan\beta = \frac{2\varphi}{1+\sqrt{1-\varphi}} \times \frac{R_s R_0}{nR_t^2}$	Theoretical	
Orzechowski	$\tan\beta = \frac{2C_d A}{\sqrt{(1+S_b)^2 - 4C_d^2A^2}}$	Theoretical	
(Chinn [107] and Moon et al. [102])	$S_b = \frac{a_0}{R_0}$ = Air core diameter at the injector exit/Injector diameter		
Fu et al. [71]	$\tan\beta = 0.033 \times A^{0.338} \times Re_t^{0.249}$	Experimental	Open-end
Inamura et al. [57,58]	$\tan\beta = \frac{k}{\sqrt{1-k^2}}$	Theoretical	
	$\beta_r = \beta\frac{a}{\sqrt{\frac{L}{R_t}\cos\beta}}exp\left(-\frac{b}{Re}\right)$		
	$a = 18.9$, $b = 670$, $k = \frac{D_{at}}{D_0}$		
	D_{at}: Air core diameter at the axial position of the tangential ports		
	β_r: Spray half angle at a distance L to the injector exit		
	h_t: Film thickness at the axial position of the tangential ports		
Rizk and Lefebvre (Ma [70], van Banning et al. [109] and	$2\beta = 6\left(\frac{A_t}{D_s D_0}\right)^{-0.15}\left(\frac{\Delta P_l D_0^2 \rho_l}{\mu_l^2}\right)^{0.11}$	Experimental	Converge-end
Khil et al. [43,44])	$2\beta = 6K^{-0.15}\left(\frac{\Delta P_l D_0^2 \rho_l}{\mu_l^2}\right)^{0.11}$		
Benjamin et al. [69,70]	$2\beta = 9.75\left(\frac{A_t}{D_s D_0}\right)^{-0.237}\left(\frac{\Delta P_l D_0^2 \rho_l}{\mu_l^2}\right)^{0.067}$	Experimental	Converge-end

1.2.5 Energy Needed for Ignition of Fluids

Table 1.3 - Properties of gaseous (normal) hydrogen [13]

Reference temperature	68 °F/528 °R	293 K
Standard pressure (1 atm) psia	14.69 psia	101.325 kPa (abs)
Density (at 528 °R and 1 atm)	0.00523 lb/ft^3	83.7 g/m^3
Specific volume (at 528 °R and 1 atm)	191.4 ft^3/lb	0.0119 m^3/g
Specific heat	Cp = 3.425 Btu/lb-R	Cp = 14.33 J/g-k
	Cv = 2.419 Btu/lb-R	Cv = 10.12 J/g-k
Velocity of sound	4246 ft/sec	1294 m/sec
	Low = 51596 Btu/lb	Low = 119.93 kJ/g
Heat of combustion	High = 61031 Btu/lb	High = 141.86 kJ/g
Flammability limits		
Hydrogen-air mixture	Lower = 4.0 vol%	Upper = 75 vol%
Hydrogen-oxygen mixture	Lower = 4.0 vol%	Upper = 95 vol%
Explosive limits		
Hydrogen-air mixture	Lower = 18.3 vol%	Upper = 59 vol%
Hydrogen-oxygen mixture	Lower = 15.0 vol%	Upper = 90 vol%
Minimum spark ignition energy at 1 atm		
In air	1.9×10^{-8} Btu	0.02 mJ
In Oxygen	6.6×10^{-9} Btu	0.007 mJ

Hydrogen and Oxygen have a low energy requirement for ignition at low temperatures. Table 1.3 shows that the mixture requires 0.007 mJ to start at atmospheric pressures. Considering this, the energy needed to be injected into the chamber by the laser must be higher than this. The proposed laser can produce 16mJ and this is more than enough to start a reaction.

1.3 Project Proposal

1.3.1 Project Goals

The goal of this paper is to show a conceptual injector design that can achieve ignition through a laser. This shows that the coaxial injector can atomize the spray and atomize the fluids injected. Compared to the engines developed prior where the laser is integrated on the side [6], this one will feed from the top at an angle and hit an area where the fuel and oxidizer have mixed to cause ignition.

1.3.2 Methodology

The proposed methodology for this project is to take the method of ignition already proven with a Q- Switched Nd:YAG (Neodymium-doped yttrium aluminum garnet) laser source and

integrate it into a coaxial injector design.. The overall structure will use common manufacturability methods and the mentioned laser source. The project will not get into changing or developing the physics of laser ablation or laser architecture design such as optics as it is out of the scope of the concept. The proposed gas and liquid species will be LOX (Liquid Oxygen) and H2 (Hydrogen Gas).

2 Injector Design

2.1 Injector Element Choice

When choosing the element pattern choice, there are some considerations to be made. The main goal is to allow the laser and the fuel to focus and atomize in a manner where the laser can then cause the ignition after hitting the mixture. As such a concentric tube with a swirler, as used in Table 1.1 will be used. This method has been used in older designs in Russian spacecraft [11] and as such is a reliable option. This is also known as a coaxial design as the injector will be generating a tangential velocity to the fuel and oxidizer fluid to allow open at the end of the injector.

2.2 Injector Element Desing Basis

Table 2.1 - Feed chamber conditions for laser ignition source [14]

Feed/Chamber Condition	Average Value
Oxygen feed pressure, $p_{f_{ox}}$	2.5 bar
Oxygen feed temperature, $T_{f_{ox}}$	90 K
Hydrogen feed pressure, p_{GH2}	12 bar
Hydrogen feed temperature, T_{GH2}	224 K
Liquid oxygen injection velocity v_{ox}	8 m/s
Gaseous hydrogen Mach number, M_{GH2}	2.8
Gaseous hydrogen flow speed at $M_{GH2} = 2.8$, v_{GH2}	3206 m/s
Velocity ratio (fuel/oxidiser), v_R	407
Gaseous hydrogen flow sonic speed, v_{GH2_s}	1145 m/s
Chamber pressure prior to priming, p_{cc_1}	approx. 20-75 mbar
Chamber pressure prior to ignition - LOx/GH2, p_{cc_2}	450 mbar
Steady state combustion pressure p_{cc_3}	1.5-1.7 bar

Table 2.2 - Experimental injector geometry [14]

Injector Geometry	
LOx post innter diameter, d_0	2.4 mm
LOx post outer diameter, d_1	3.2 mm
H2 outer diameter, d_2	6.0 mm
CH4 outer diameter, d_2	5.0 mm
Fuel sonic nozzles diameter, d_{snl}	2.0 mm

Table 2.1 and Table 2.2 shows the feed conditions that contributed to ignition in the combustion chamber. The injector will aim to have the same temperature and conditions as the laser used for low-temperature settings where the fuel and oxidizer have a high ignition energy requirement. [14] Similar geometry on the exit conditions will be used but because of the tangential velocity introduced it will be different exit conditions (ie. pressure, velocity, and Mach number)

2.3 Spray Cone Approximation and Injector Element Design

2.3.1 Spray Cone Approximation

With the variation in spray cone angle equations, a rough approximation using Khil et al. [15, 12] and H. Lefebvre, Equation 2.1 can be made to help position the angle of the laser in the assembly. Since the area of ionization for energy is large, there is room for loss in precision and looser tolerances. Here the varying factor that will be changing will be that of the inlet pressure. The values that will be changing will be that of Area and Pressure drop. Where the inlet pressure will increase to show a pressure drop.

$$2\theta_m = 6K^{-0.15}\left(\frac{\Delta P_L d_0^2 \rho_L}{\mu_L^2}\right)^{0.11} \tag{2.1}$$

Where,

$$K = \frac{A}{D_s d_0} \tag{2.2}$$

Using

Figures 2.1 and 2.3 show the difference in spray angles vs pressures at different K values. The K values represent an increase in the diameter of the swirl chamber vs that of the exit

diameter. Appendix D will show the varying K Values for a diameter range of 2.4 mm to 24.2 mm for LOX and 12 mm to 27.8 mm for H2. The pressure range is assumed 250000 Pa to 571200 Pa for LOX and 1200000 Pa to 1500000Pa for H2. The initial range was chosen in an assumed pressure increase to the exit value in Table 2.1 As the injector gets bigger and the K value increases, the spray angle is shown to decrease but increase as pressure increases.

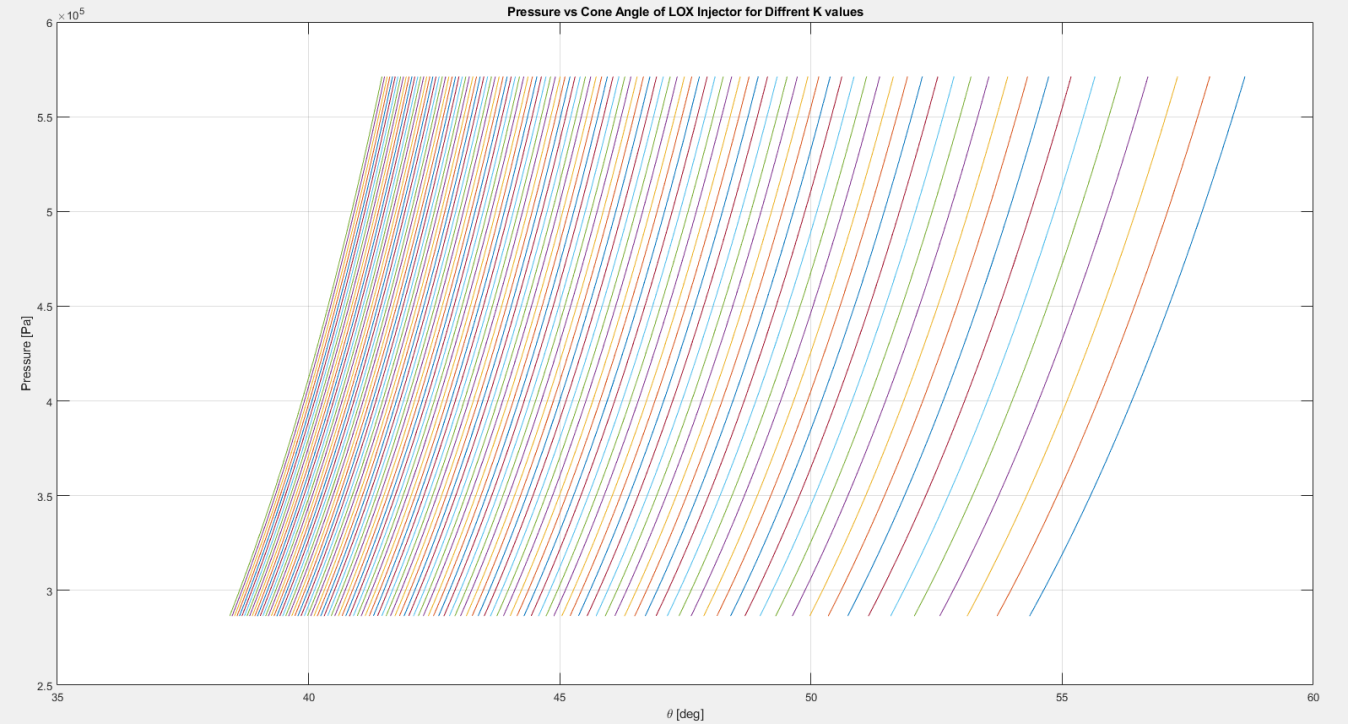

Figure 2.1 - Varying K values pressure vs spray angle (lower K values from right to left)

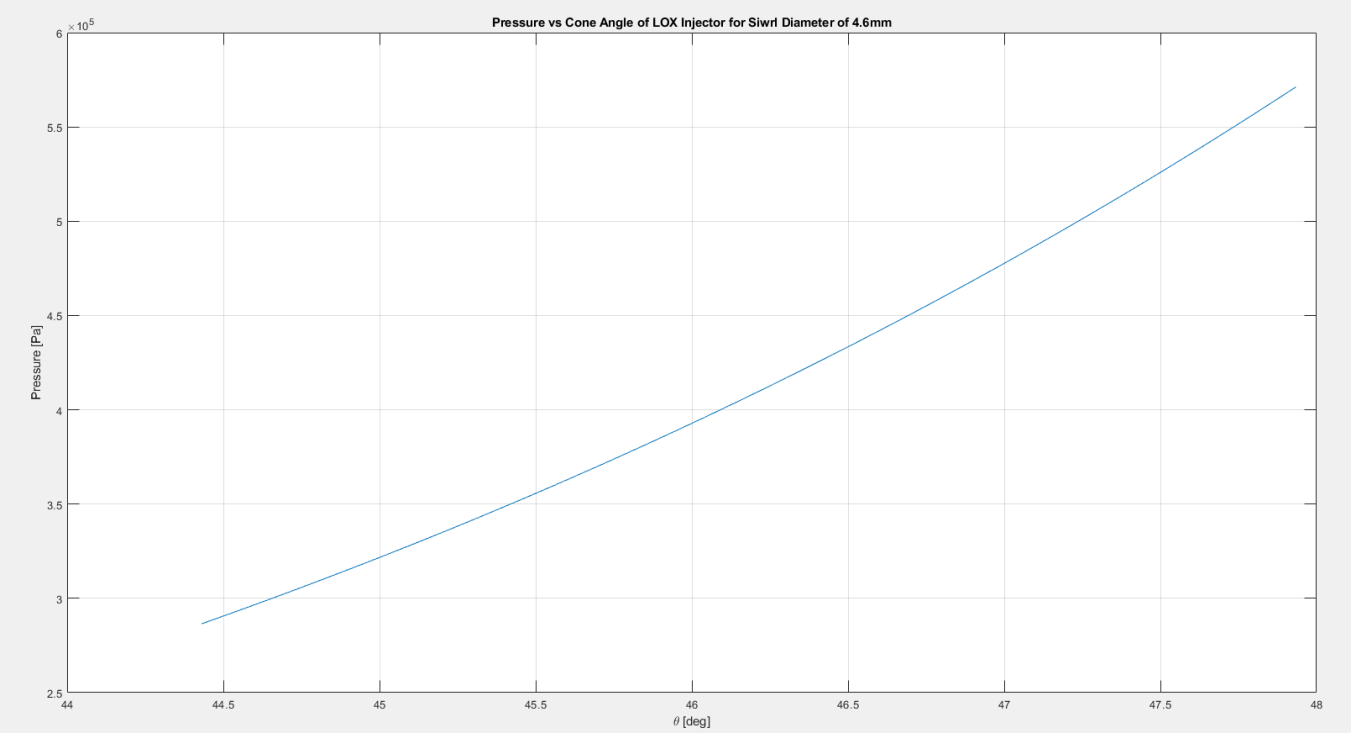

Figure 2.2 - Pressure vs cone angle of LOX injector at 4.6 mm

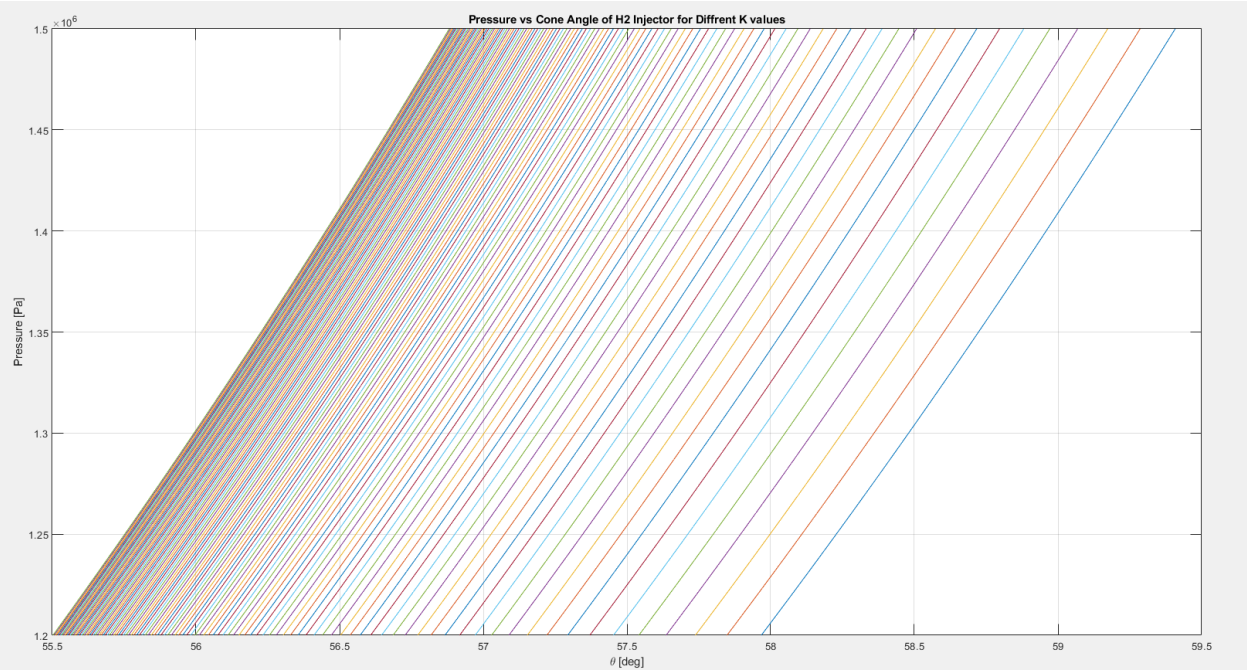

Figure 2.3 - Varying K values pressure vs spray angle for H2 injector (lower K values from right to left)

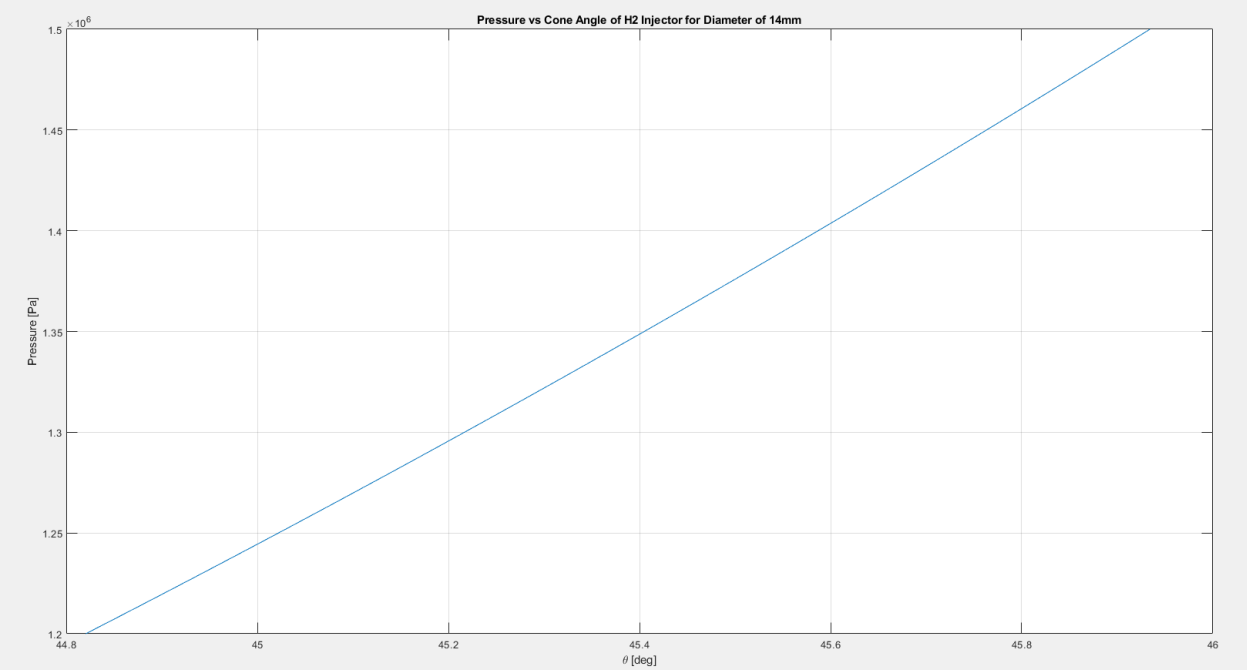

Figure 2.4 - Pressure vs cone angle of H2 injector at 14 mm

Figure 2.2 shows the spray Angle for the Lox injector at 4.8mm which is the swirl chamber that will be chosen to continue in the analysis while 2.4 shows that of the H2 injector. This is an approximation and the experimentally derived equation was for different fluids. But it should help in positioning the laser source.

2.3.2 Injector Element Design

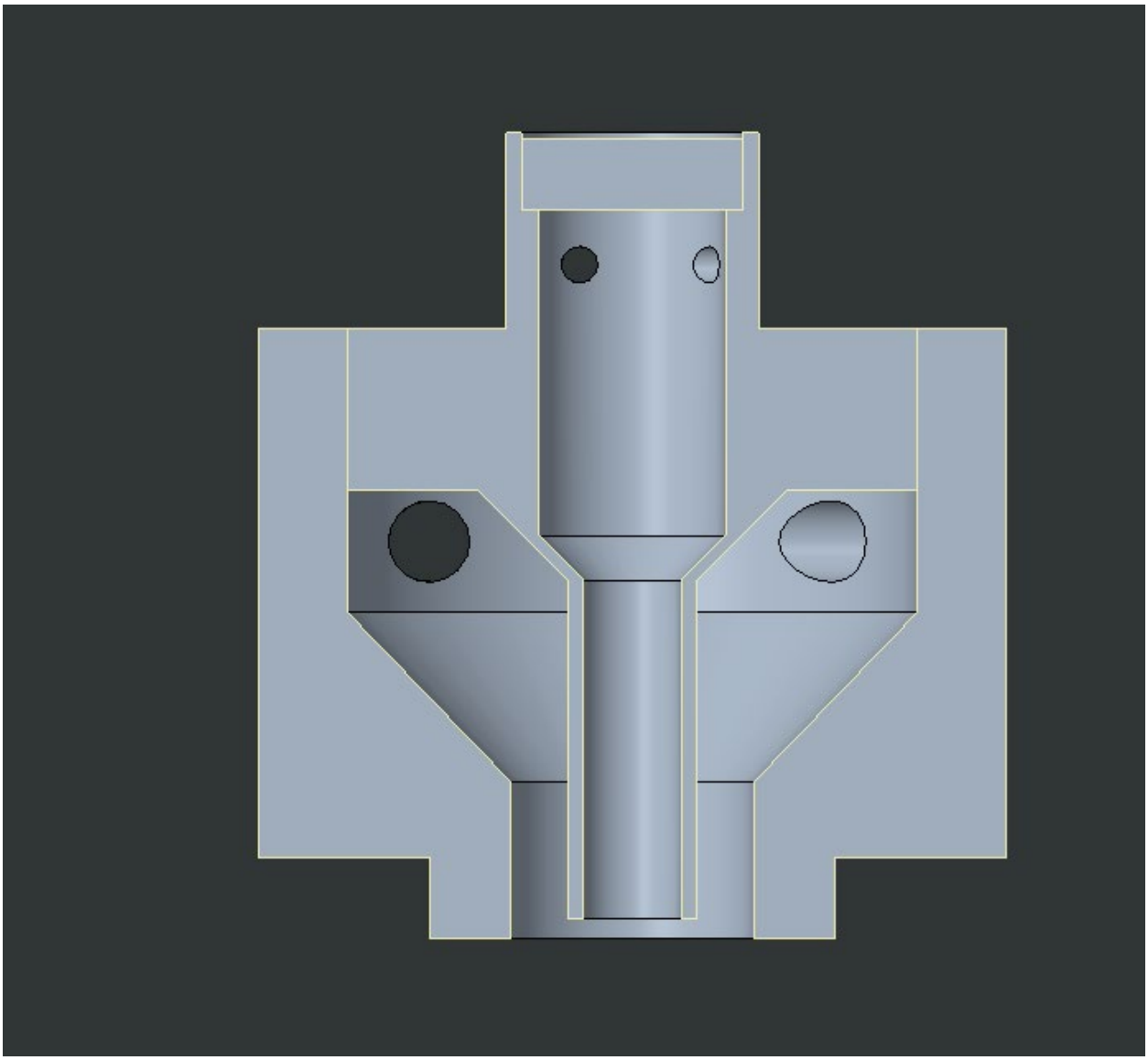

Figure 2.5 Coaxial injector element design front cross section

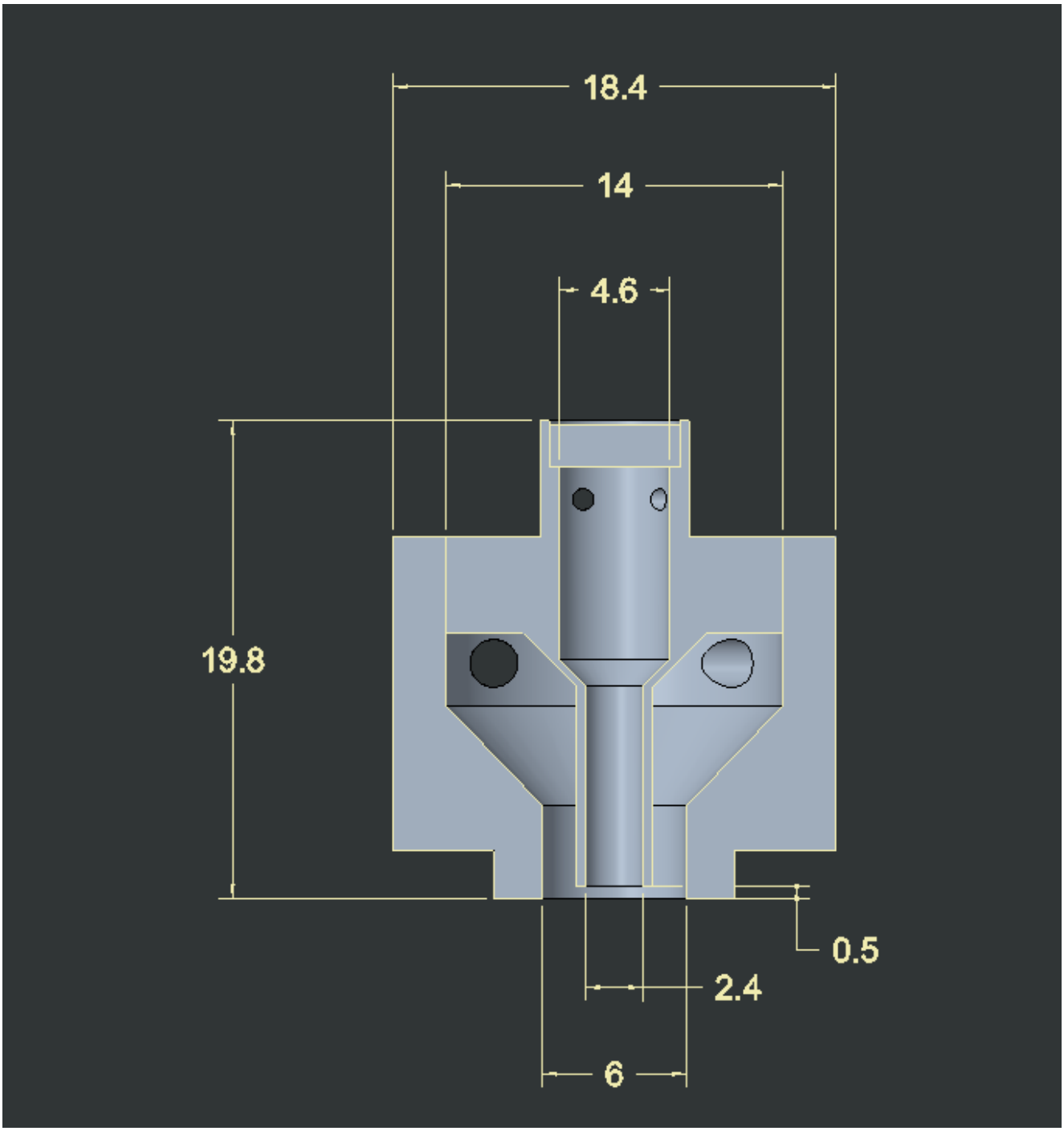

Figure 2.6 Dimensions of coaxial injector element in front cross section

As seen in Figures 2.5 and 2.6, the injector assembly consists of 3 parts. The fluid injector (center), gas injector (exterior concentric geometry), and lid to hold and seal the fluid injector. The design has holes in each of the different parts to allow for the gas and fluid to flow in with a tangential velocity. Thus, in the end, the fluid will open past the walls of the geometry and create a conical shape thus atomizing the fluid. The gas fuel mixture will expand and when ignited by the laser source trigger the start of the reaction.

Manufacturability of the parts can be done with both a CNC and Lathe machine. The process is time-consuming but to get the necessary internal and external geometry both will need to be done. The material choice is 304 SST (Stainless Steel) due to the yield strength and thermal properties of the material being high enough to withstand the conditions. As shown in Table 2.1, the conditions at the injector end are extreme. The pressure load of 12 bar (1.2 MPa) can be easily withstood by 304 SST, which has a yield stress of 2050 bar (205 MPa). Since there is also a portion where the flow after the injector will become supersonic, Stainless steel should be able to withstand this environment as well.

To assemble the structure, micro-welds will be used on the top and in between each section to keep it constrained to each other. These will not only be able to hold but also provide a seal in between each section to prevent leakage and allow for a stable pressure environment. Figure 2.7 shows the cross-section where the welds will be placed.

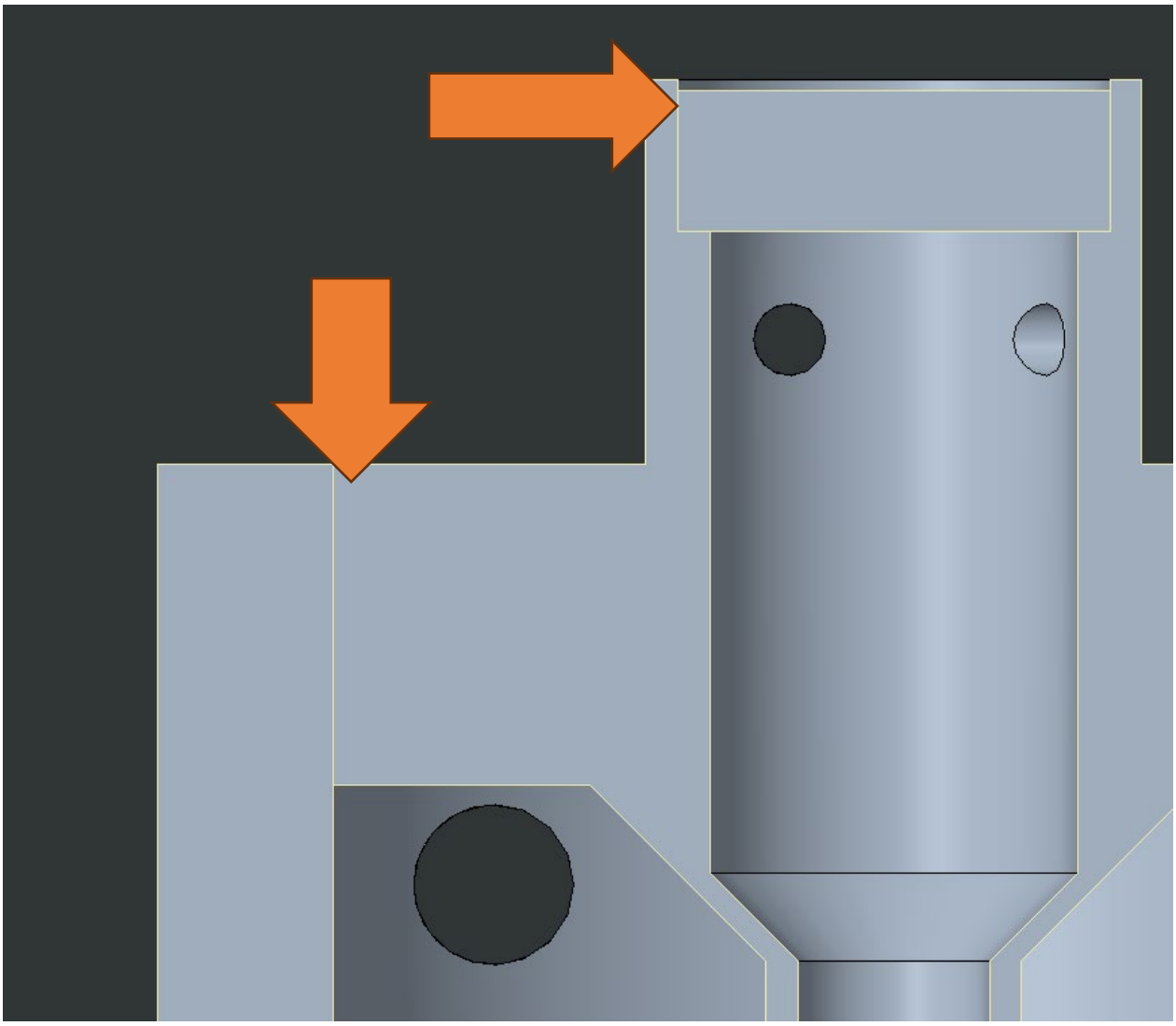

Figure 2.7 - Injector weld locations on pintle injector assembly

2.3.3 Injector Element Overall Assembly

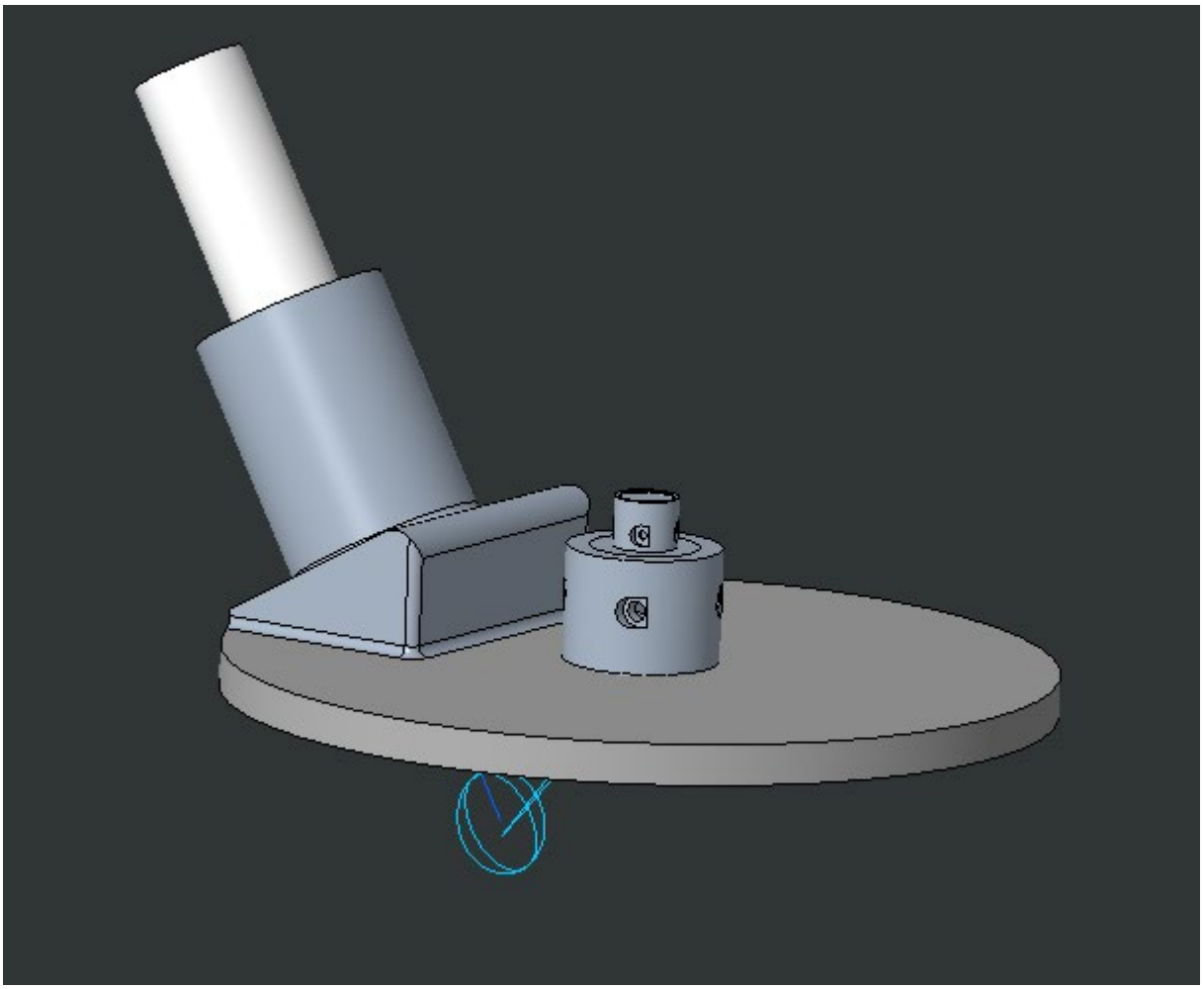

Figure 2.8 - Isometric view of laser injector assembly

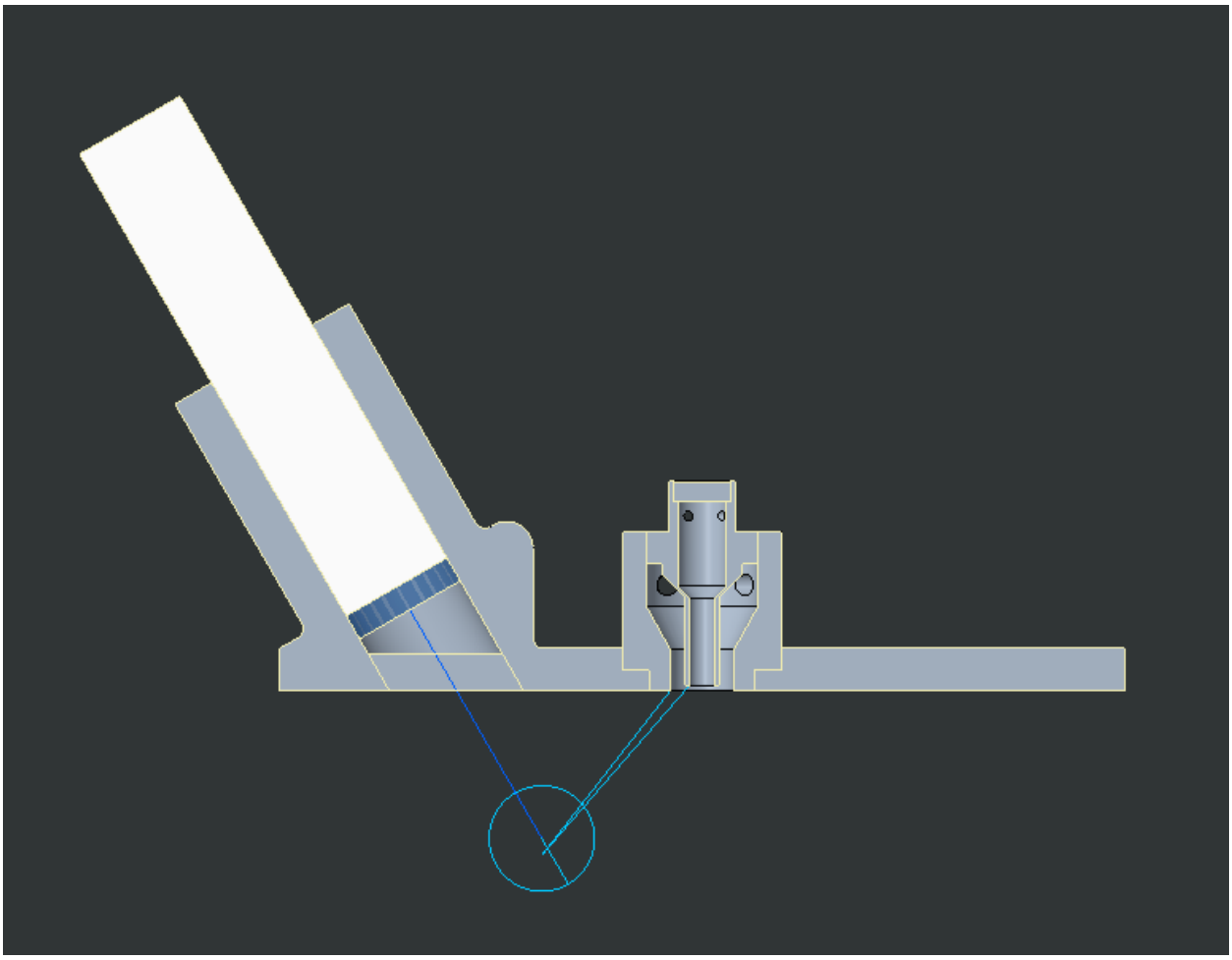

Figure 2.9 - Front cross section of injector assembly with laser source

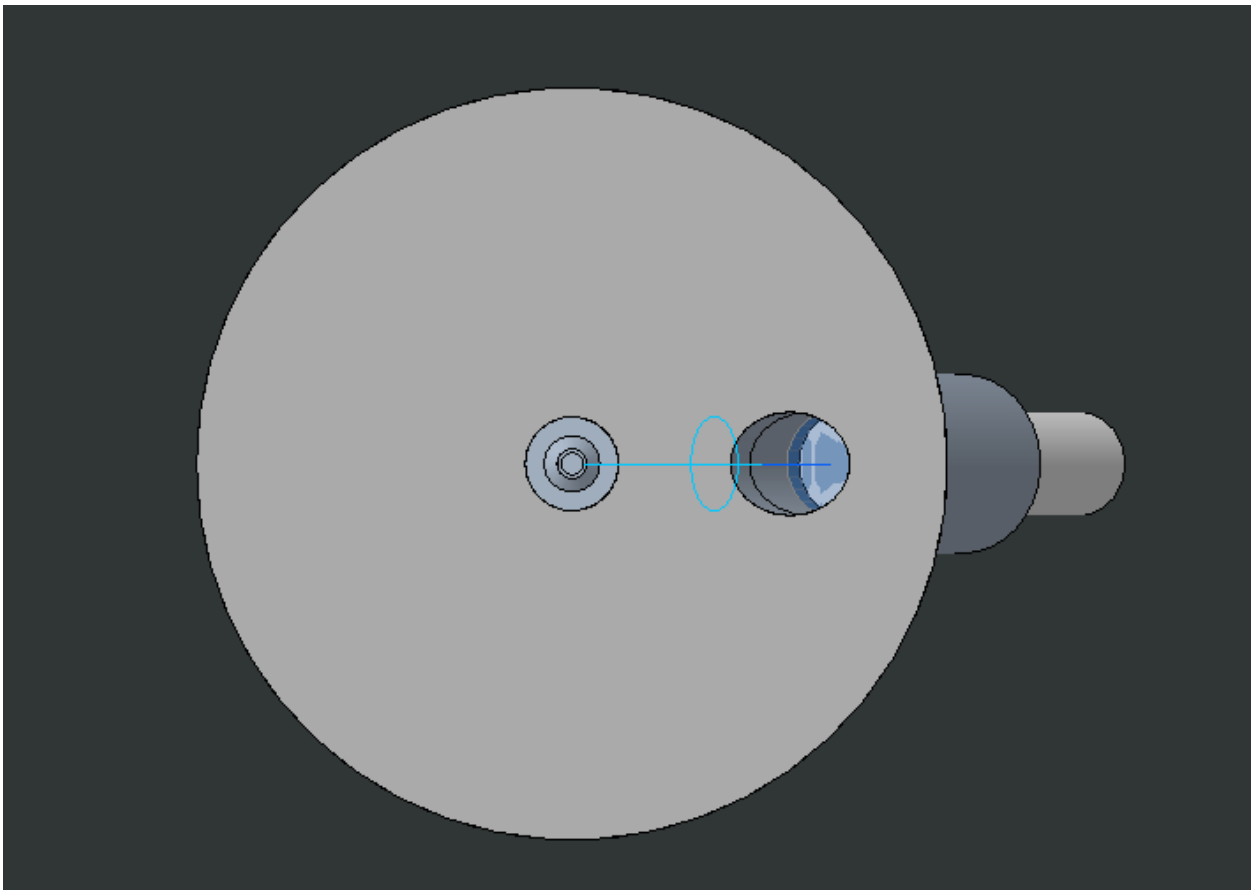

Figure 2.10 Bottom view of laser assembly with window

The overall assembly can be seen in Figures 2.8, 2.9, and 2.10. The injector assembly and the plate are held together with welds. While the laser source much like a conventional spark plug connects via an M12x1 screw thread. The blue line represents the beam path and the circle area represents the flame kernel energy deposit due to air ionization. The beam will thus cover enough space to cause an ignition when the fuel and oxidizer come into the region.

3 Computation Analysis of Coaxial Swiler Atomization

3.1 Setup of CFD Analysis

3.1.1 Geometry and Mesh

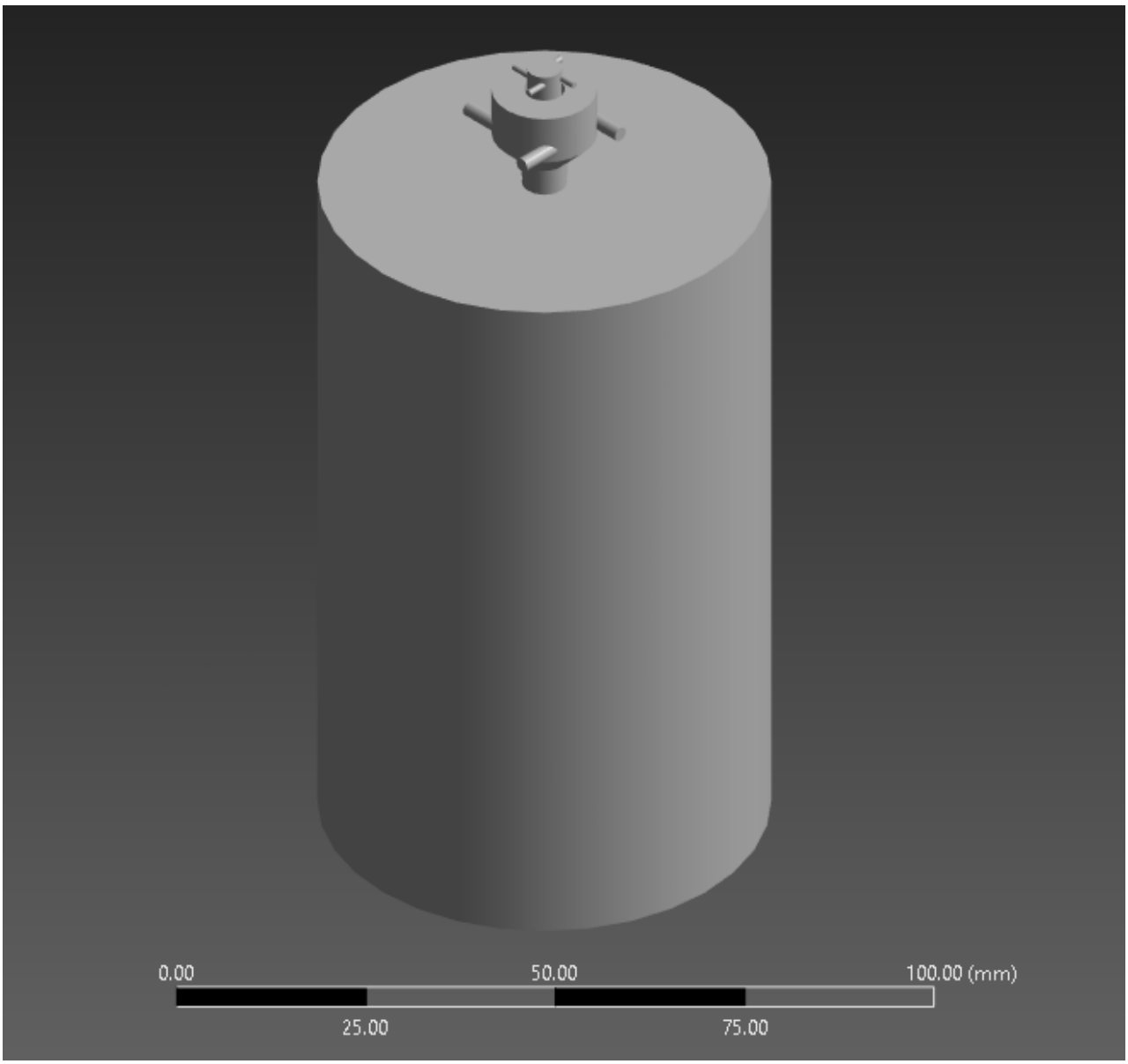

Figure 3.1 - Isometric view of CFD geometry

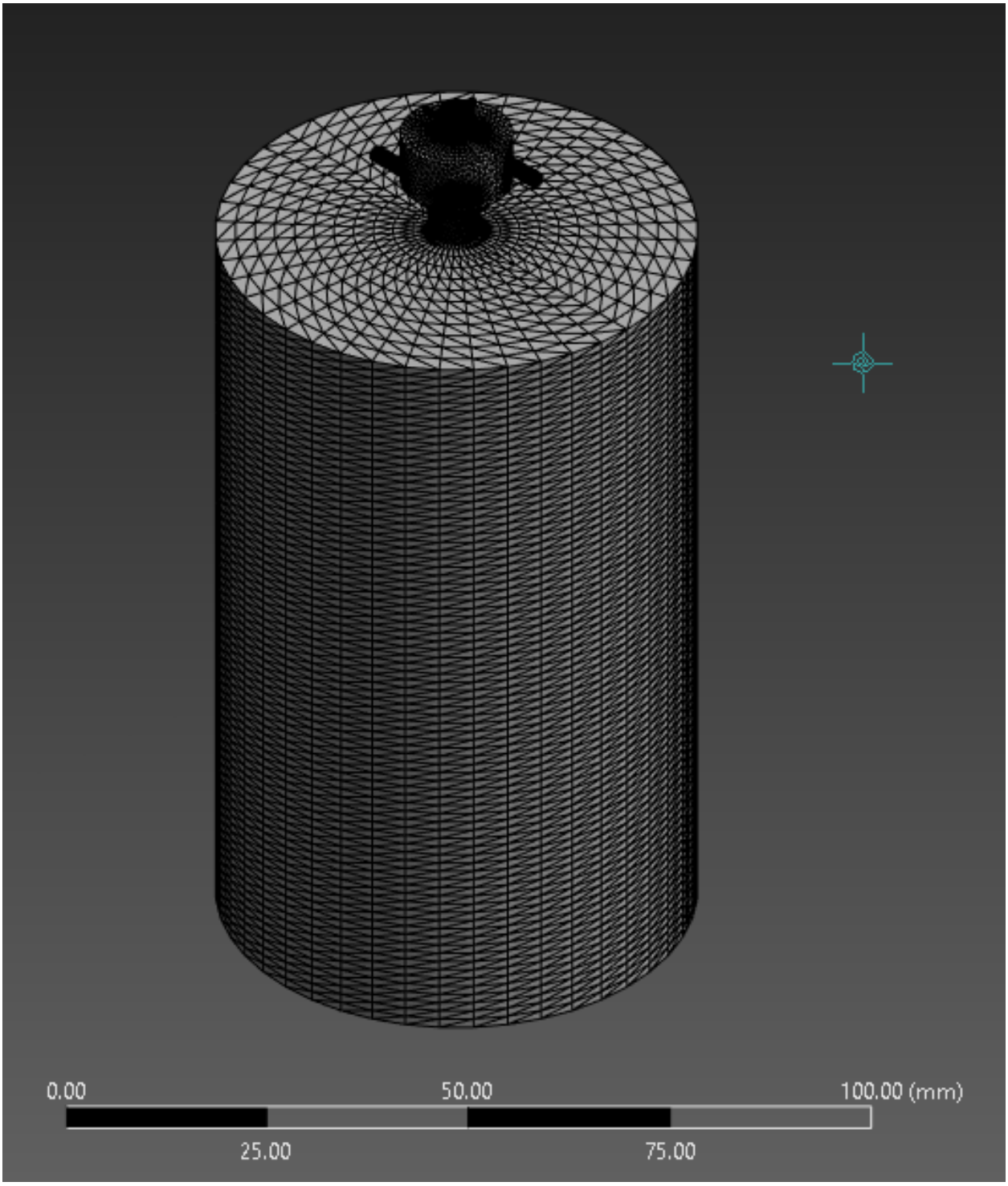

Figure 3.2 - Isometric view of mesh

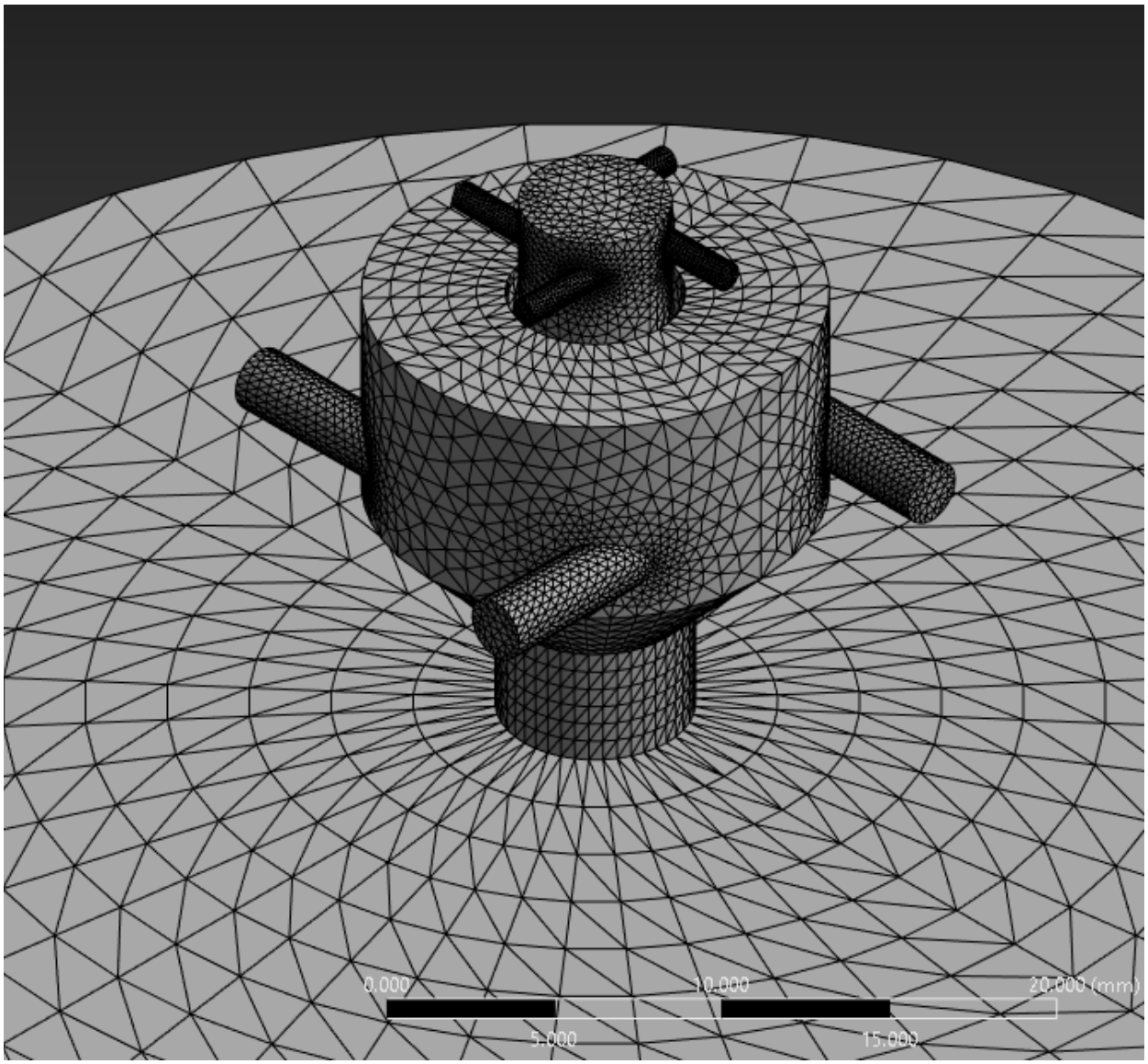

Figure 3.3 - Coaxial injector mesh

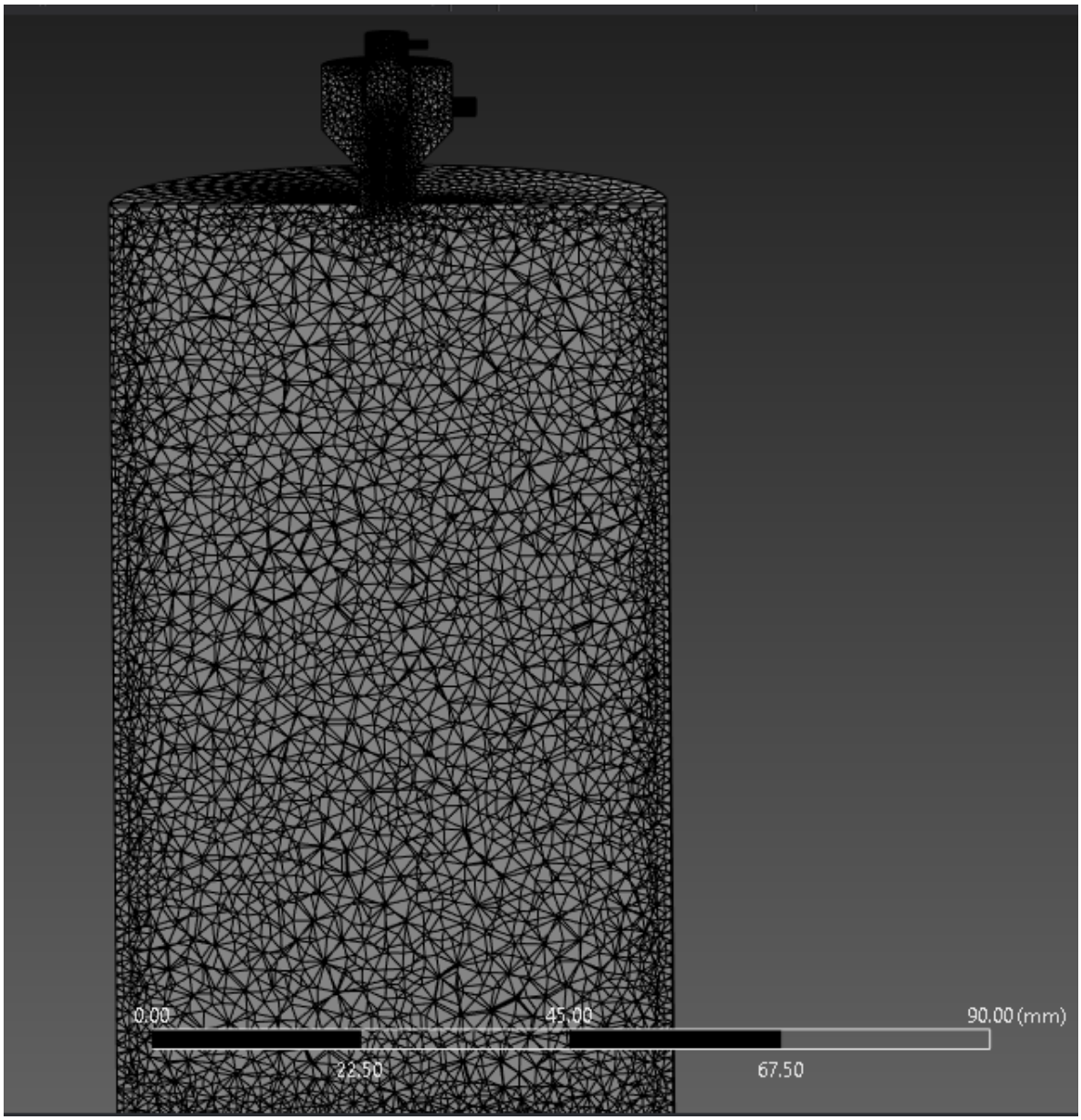

Figure 3.4 - Mesh negative geometry cross-section

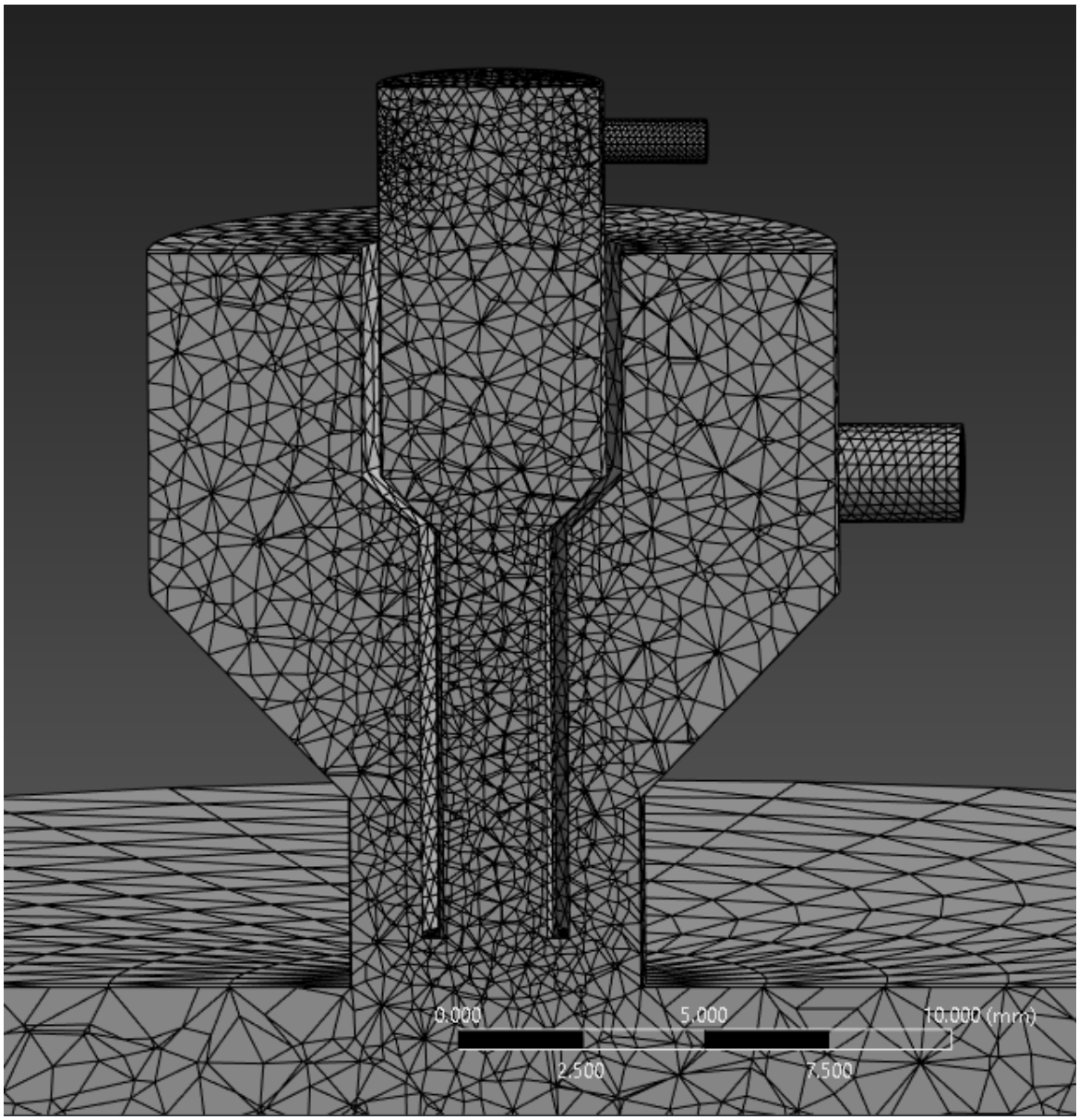

Figure 3.5 - Mesh of coaxial injector cross section

Table 3.1 - Mesh quality info

Mesh Feature	Value
Orthogonal (> 0.1 Recommendation)	.702
Skewness Average (< 0.9 Recommendation)	.302
Element Count (< 512,000 License Limitation)	470043

Figures 3.1 to 3.5 show the Geometry and Mesh of the Coaxial Injector that will be used to simulate the fluid analysis. Face meshing was used to reduce the number of elements to less than 512,000. This is under the limit of the ANSYS Student license and processing power of 4 cores. To have a good quality mesh, the values in Table 3.1 were achieved. The values are under or over the recommended industry values for skewness and orthogonal quality.

3.1.2 Simulation Set-Up and Input Parameters

The following are the changes in settings for the CFD analysis. Most of the settings were left as default. The main changes are to the operating conditions, boundary conditions, and material settings for the mixture of fluids.

Table 3.2 - General settings for coaxial injector 3D simulation

General Settings for Simulation	
Conditions	Settings
General Solver	Pressure based
Simulation State	Steady State
Velocity Formulation	Absolute
Energy Equation	On
Viscous Model	SST k-omega
Fluid Model	Ideal Gas (Hydrogen Gas and LOX)

Table 3.2 shows the general settings that were used in the model. A pressure-based model was used as we are assuming an incompressible flow. A steady-state model was used as time was not a considered factor. SST k-omega was used as the default solver and the fluid was changed to ideal gas for the mixture.

Table 3.3 - Species transport settings for gaseous H2 and LOX

Species Transport Settings	
Condition	Settings
Volumetric	On
Eddy – Dissipation	On
Diffusion Energy Source	On
Boundary Species	H2 and O2<l> (liquid)

Species transport was used to include the fuel and oxidizer mixture. The energy Equation turns on as this is also used in combustion modeling. While no combustion is occurring due to the environmental conditions being on the low. The energy needed, 0.007 mJ at low temperatures (293 K), to ignite the fluid mixture will thus be from the laser source [13].

Table 3.4 - Material mixture (boundary species) settings

Material Mixture Settings (Boundary Species)	
Condition	Settings
Reaction	$2H_2 + O_2 \rightarrow H_2O + Energy$
Density	Ideal Gas

The material mixture condition was changed to allow LOX to be part of the mixture rather than the oxygen gas.

Table 3.5 – Changed boundary conditions and operating conditions

Boundary Condition Settings	
Condition	**Settings**
Operating Conditions	
Operating Pressure [Pa]	**0**
H2 Inlet Mass Flow Inlet	
Mass Flow [kg/s]	0.0076
Gauge Pressure [Pa]	1251200
Total Temp [K]	224
Mass Fraction	0.17
LOX Mass Flow Inlet	
Mass Flow [kg/s]	0.0413
Gauge Pressure [Pa]	258560
Total Temp [K]	90
Mass Fraction	0.83
Pressure Outlet	
Gauge Pressure [Pa]	101325

Table 3.5 shows the settings that were changed based on the conditions from Tables 2.1 and 2.2, as well as the calculated mass flow rate from the exit of the injector for each of the injector elements. Operating Pressure was set to zero to allow the gauge pressure to be accurate and not consider absolute pressure in Ansys. Mass fractions were set to the calculated values from CEA (Appendix B) for a mixture ratio of 5 for the fuel/oxidizer mixture. The operating pressures that are inputted should also give a 45 deg for H2 and 44 deg spray cone angle for the LOX base don Figures 2.2 and 2.4.

Table 3.6 - Solution and calculation settings

Solution Method and Calculation	
Condition	Setting
Solution	Coupled
Gradient	Least Squared Cell-Based
Spatial Discretization	Second Order or Second Order Upwind
Initialization	Hybrid
Number of Iterations	250

The solution method was left to the default setting of coupled. Initialization was changed to hybrid to allow for the solver to calculate the starting conditions. The number of iterations was 1200 to allow for the solver to converge.

3.2 Results of CFD Analysis

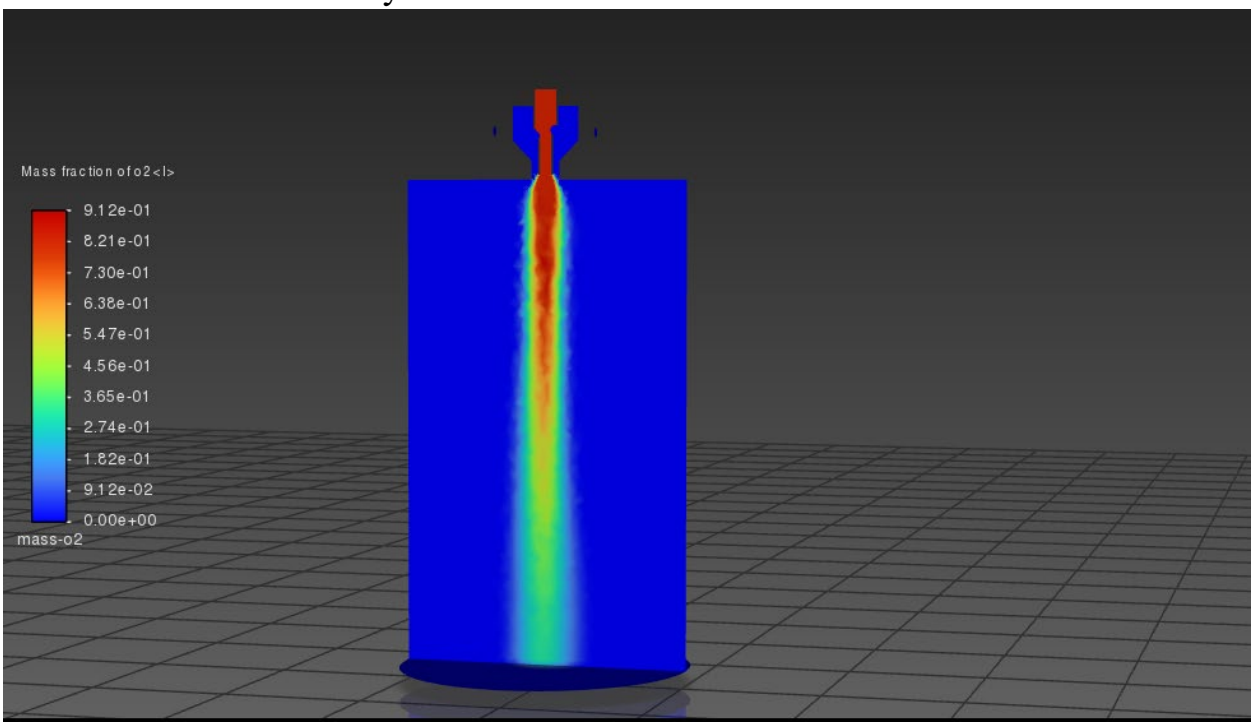

Figure 3.6 - Mass fraction contour of LOX from injector

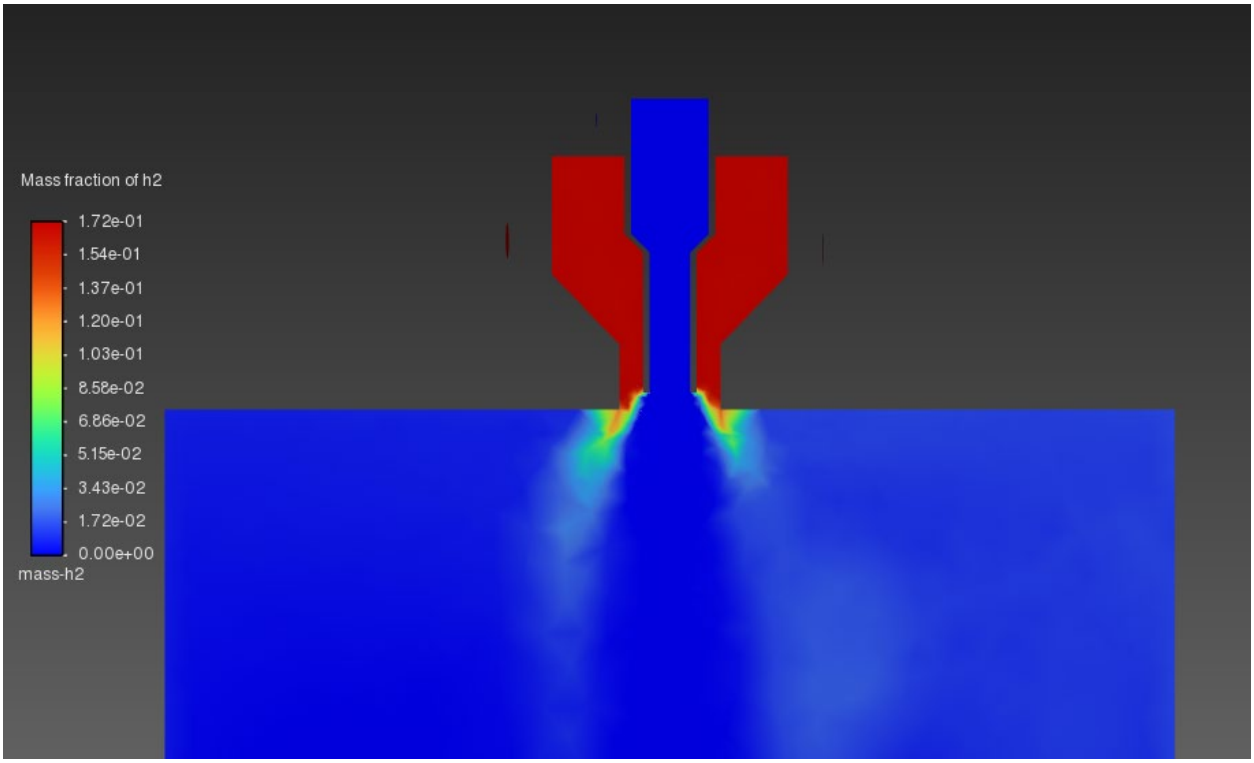

Figure 3.7 - Mass fraction contour of H2 gas from injector

Figures 3.6 and 3.7 show the atomization and spray geometry of the fluids from the injector. The angle of injection is larger than the estimated 44 deg visually. But for LOX, it is less than the estimated 52 deg. This does not however make the ignition impossible as the large kernel size can still react with the mixture.

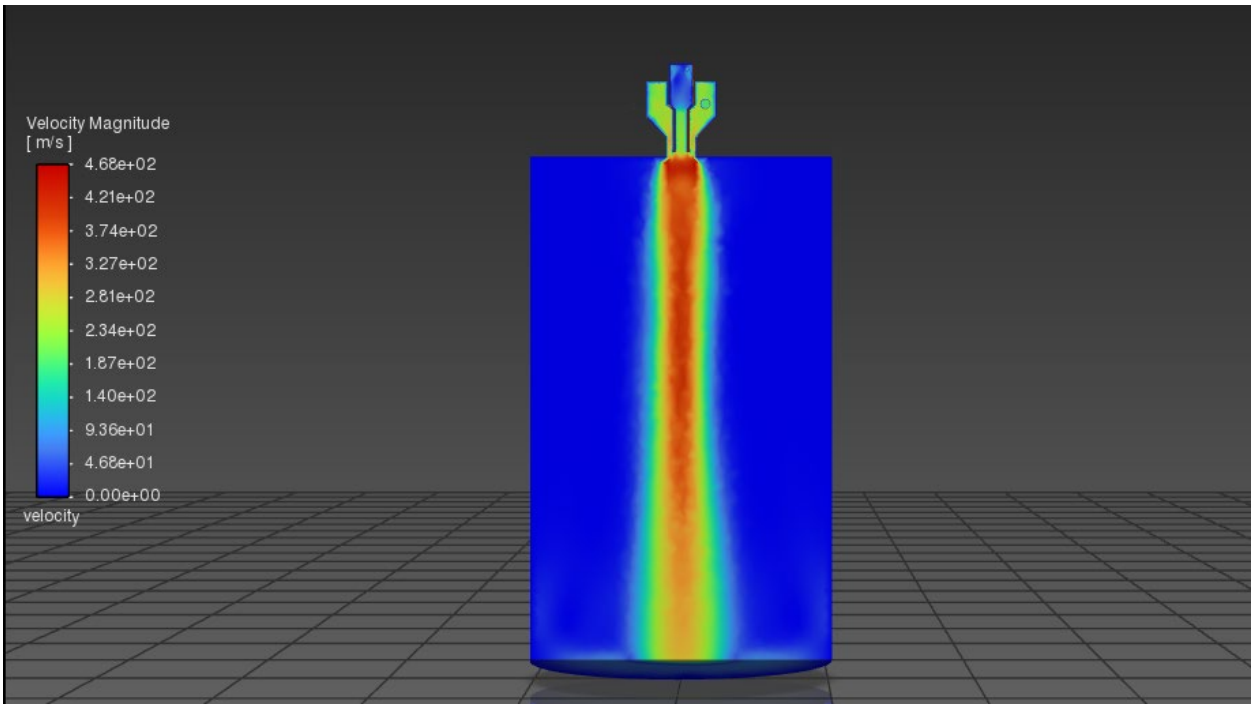

Figure 3.8 - Velocity contour of fluid from injector

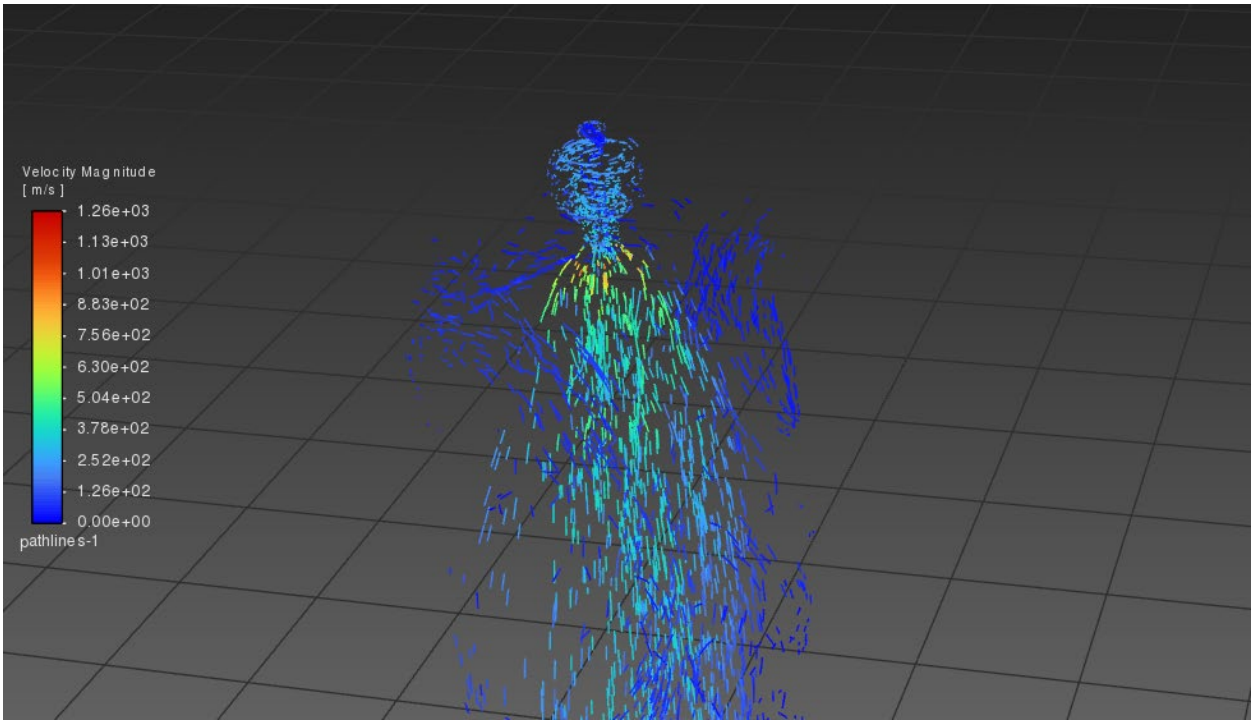

Figure 3.9 - Velocity pathlines of coaxial injector showing tangential velocity

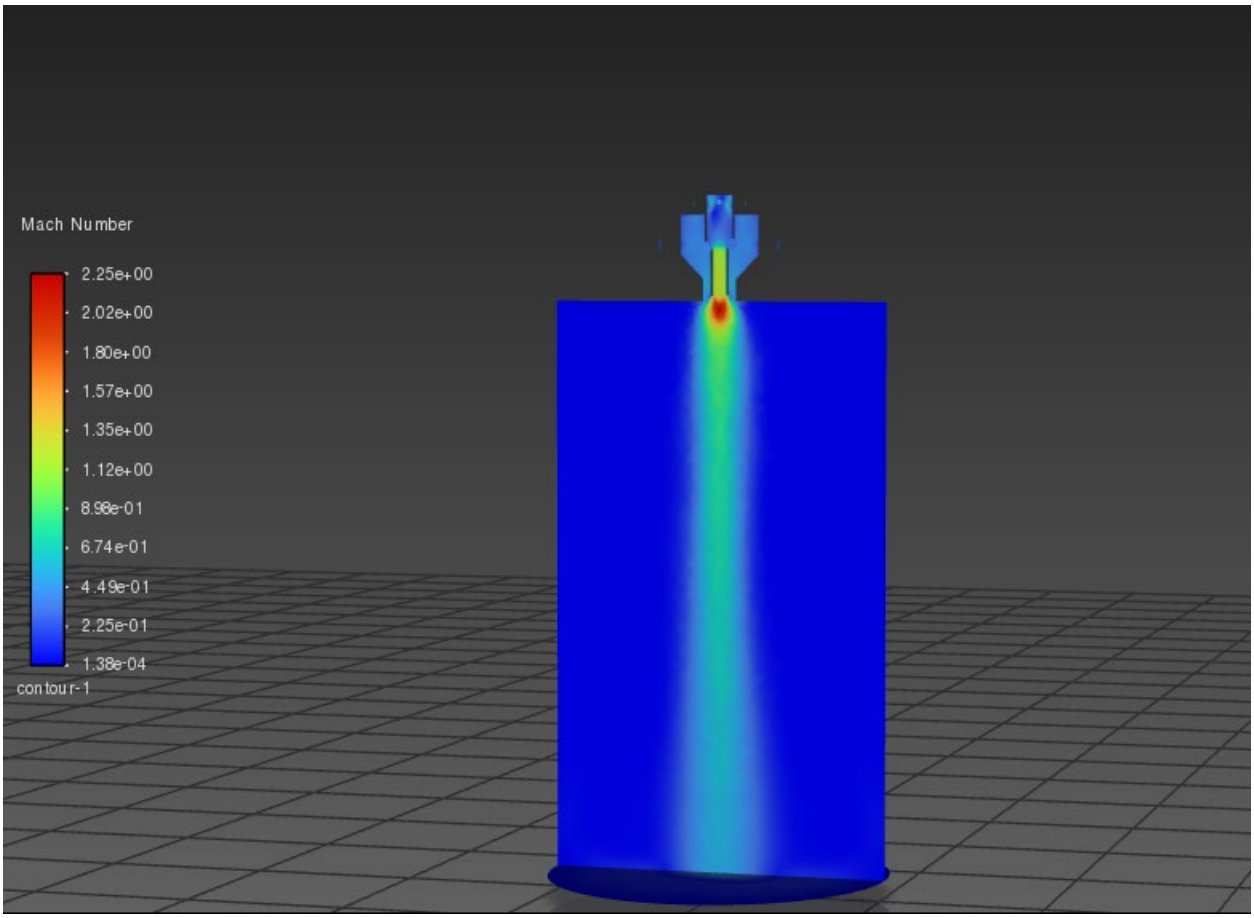

Figure 3.10 - Mach number contour

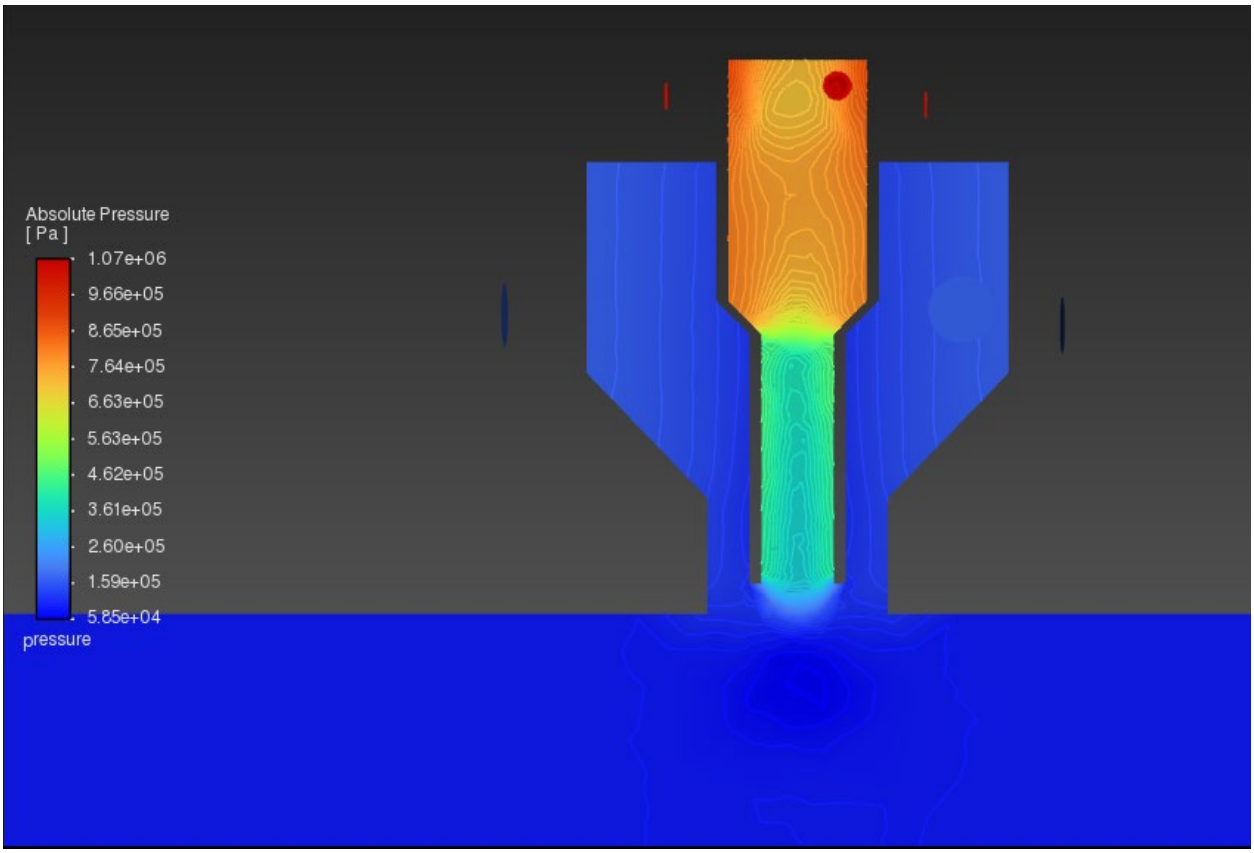

Figure 3.11 - Pressure inside injector

Figures 3.8 and 3.9 show the velocity in and outside the injector going into the combustion chamber. Inside the injector for both H2 and LOX, there is a tangential velocity that causes the expansion as it leaves the injector. As the area decreases, the velocity increases as it leaves the injector into the combustion chamber and pressure decreases Figure 3.11. At the center of the LOX injector, one can also see the low-pressure swirl effect take place due to the tangential velocity. The velocity of H2 leaving the injector is around 1100 m/s while LOX leaves at 300 m/s. This roughly translates to Mach 1.2 for H2 and 2.5 for LOX leaving the injector as seen in Figure 3.10.

3.3 Comparison of Results to Similar Designs

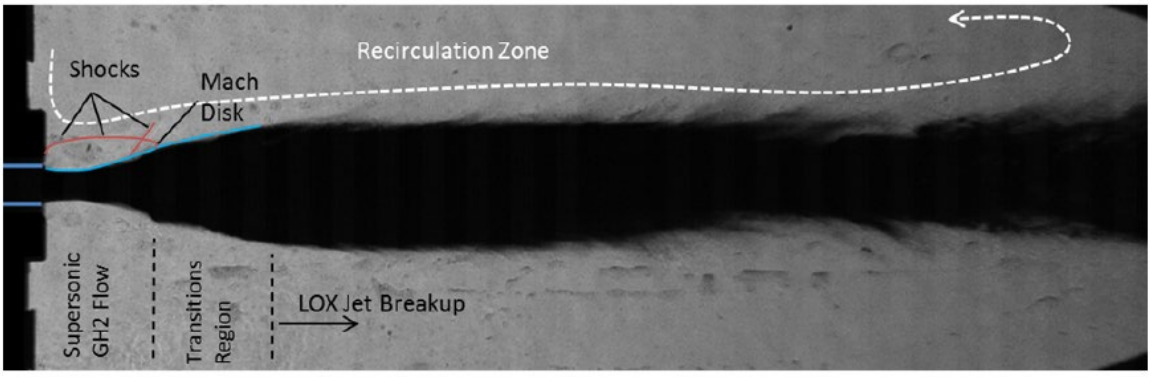

Figure 3.12 - Spray image prior to ignition [14]

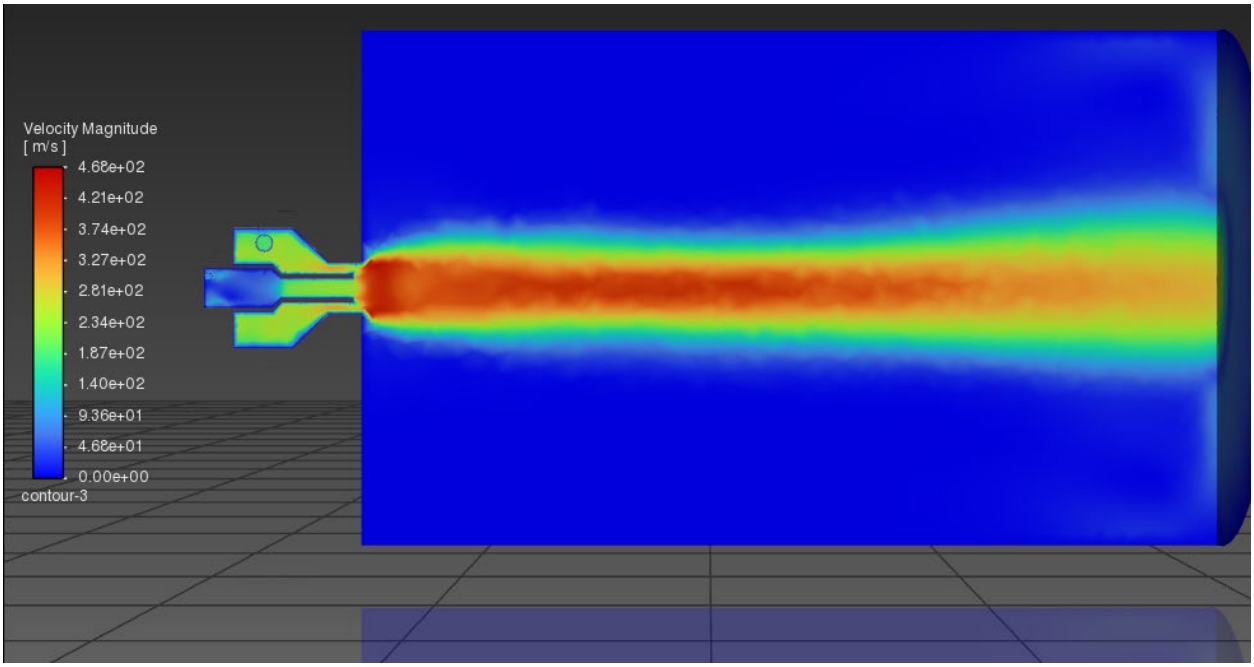

Figure 3.13 - Side velocity contour

Comparing both Figure 3.12 and 3.13 there are similarities in the spray of the fluid from the injector. The fluid breaks up to break up the fluid and is present. Some differences are the velocities of the mixture. While Manfletti and Kroupa [14] have velocities of 1145 m/s and 8 m/s for H2 and LOX respectively, this design gets speeds of 345 m/s and 378 m/s for both of the fluids. This also changes the Mach number in where this design achieves 1.6 at the exit of the Lox injector rather than a higher Mach at the H2 injector.

Another similarity yet also different is the expansion of the fluid mixtures going into the chamber. In Figure 3.12, the expansion of the fluid happens after the shock waves upon the existing chamber. In Figure 3.13, it happens almost immediately after exiting the chamber. This is most likely due to the absence of shock waves due to the H2 but instead happening in the LOX injection. These shockwaves are wave could be causing the H2 as seen in Figure 3.7 to expand more than the estimated spray cone angle. These shock waves are difficult to see in the CFD analysis and would need to be done in a transient solver rather than a steady state to capture the pressure differentials. So, this is a hypothesis as to why this is occurring.

4 Discussion

The objective of this design was to make an injector that has a laser come in from above rather than needing a window in the combustion chamber. By investigating the fluid atomization and properties as it was injected, the possibility of using a fixed location of ionized air can be determined. The results show that the injector can accomplish the automation and dispersion of LOX and H2 into the chamber in a flow pattern where a 10 mm-sized kernel can deliver the needed energy to cause ignition.

5 Future Development

For continued development, observation of shockwaves that are created by the fluid being injected into the chamber should be studied. With the current analysis being done in a steady-state solver, the shockwaves were not visible. As such this would be a good method to understand the flow pattern better and where to deposit the kernel of energy where pressure differences would not cause issues.

While in a transient solver, one can also possibly simulate the properties of such a flame kernel using the ANSYS spark ignition available in species transport combustion. This could determine if the deposition of air is viable with the environmental factors of pressure and fluid flow.

In commercial rocket engines, there is also not one but multiple injectors, that are present in the manifold. As such incorporating a multi-injector design pattern would be the next step in seeing how the fluid disperses and interacts with other streams.

6 Conclusion

After reviewing the CFD analysis and injector design, the fluid flowing into the combustion chamber is atomized and dispersed in a way where a deposited energy can cause an ignition. This means that direct laser ignition rather than laser ablation could work but further study needs to be conducted to see how the deposition of energy is affected by the environment. The ignition of rocket engines has been done the issues in an ablative laser design have been documented as a possibility but the infrastructure involves big laser architecture. Incorporating a system where it is miniaturized and not sacrificing performance can lead to a more commercially reliable option for ignition.

7 References

[1] Pletnev, N. V., Ponomarev, N. B., Motalin, G. A., and Murashov, V. F., “Development and testing of the laser system of ignition of rocket engines,” *Combustion, Explosion, and Shock Waves*, vol. 56, 2020, pp. 181–187.

[2] Kroupa, G., and Börner, M., “A miniaturized high energy laser for ignition of rocket engines,” *International Conference on Space Optics — ICSO 2018*, 2019. https://doi.org/10.1117/12.2536117

[3] O’Briant, S. A., Gupta, S. B., and Vasu, S. S., “Review: Laser ignition for aerospace propulsion,” *Propulsion and Power Research*, vol. 5, 2016, pp. 1–21. https://doi.org/10.1016/j.jppr.2016.01.004

[4] Loktionov, E. Y., and Pasechnikov, N. A., “First tests of laser ignition in wankel engine,” *Journal of Physics: Conference Series*, vol. 1787, 2021, p. 012031. https://doi.org/10.1088/1742-6596/1787/1/012031

[5] Börner, M., Manfletti C., Oschwald M., “Laser Re-Ignition of a Cryogenic Multi-Injector Rocket Engine”, 6 TH EUROPEAN CONFERENCE FOR AERONAUTICS AND SPACE SCIENCES (EUCASS), July 2015

[6] Hilton, D. K., and Van Sciver, S. W., “Absolute dynamic viscosity measurements of subcooled liquid oxygen from 0.15MPA to 1.0MPA,” *Cryogenics*, vol. 48, Jan. 2008, pp. 56–60. https://doi.org/10.1016/j.cryogenics.2007.11.002

[7] Taira, T., “High brightness microchip lasers for engine ignition,” *Frontiers in Optics 2012/Laser Science XXVIII*, 2012. https://doi.org/10.1364/FIO.2012.FM3G.1

[8] Zambalov, S. D., Yakovlev, I. A., and Skripnyak, V. A., “Numerical simulation of hydrogen combustion process in rotary engine with Laser Ignition System,” *International Journal of Hydrogen Energy*, vol. 42, 2017, pp. 17251–17259. https://doi.org/10.1016/j.ijhydene.2017.05.142

[9] Ronney, P. D., “Laser versus conventional ignition of flames,” *Optical Engineering*, vol. 33, 1994, p. 510. https://doi.org/10.13140/2.1.1845.1206

[10] Manfletti, C., Oschwald, M., & Sender, J. (2009). *Theoretical and Experimental Discourse on Laser Ignition in Liquid Rocket Engines*. The 27th International Symposium on Space Technology and Science, July 2009

[11] Gill, G. S., Nurick, W. H., Keller, R. B., and Douglass, H. W., "*Liquid rocket engine injectors"*, NASA SP-8089, March 1976.

[12] Kang, Z., Wang, Z., Li, Q., and Cheng, P., "Review on pressure Swirl Injector in liquid rocket engine," *Acta Astronautica*, vol. 145, Apr. 2018, pp. 174–198. https://doi.org/10.1016/j.actaastro.2017.12.038

[13] NASA, " Glenn Safety Manual – Chapter 6, Hyrdogen", NASA GLP-QS-8715.1.6, November 2024

[14] Manfletti, C., and Kroupa, G., "Laser ignition of a cryogenic thruster using a miniaturised nd:YAG laser," *Optics Express*, vol. 21, 2013. https://doi.org/10.1364/OE.21.0A1126

[15] Lefebvre, A. H., "Properties of sprays," *Particle & Particle Systems Characterization*, vol. 6, Jan. 1989, pp. 176–186. https://doi.org/10.1002/ppsc.19890060129

Appendix A – MATLAB Calculations for K Constant Graphs

```
%% Cone Angle Approximation

clc, close all, clear all

%% Lox Angle Approximations

% Geometry Values

d0 = 2.4; %[mm] Lox exit diameter


rLox = (1.2:.1:12.1); %[mm] Diameter of 2.4 to 24.2 mm for input of injector. Divided by 1000 for meters conversion

rLoxmeter = rLox/10^3; % Conversion to meters

A0Lox = pi*rLoxmeter.^2; % Area of Changing swirl chamber (H2 calcs)


A_LOX = pi*rLoxmeter.^2; % Area of Changing Swirl chamber

Ds_LOX = rLoxmeter; % Diameter changing swirl chamber

do_LOX = (d0*2)/10^3; % Diameter of injector exit


muLOX = 0.0001956; % dynamic viscosity of LOX


KLOX = A_LOX./(Ds_LOX.*do_LOX); %K constant calculation


for i=1:1:length(KLOX)


    PlLOX = 250000:571200; % Pressure Range


    rhoLox = 1141; %kg/m^3

    thetaLOX = (6*KLOX(i).^-0.15.*((PlLOX.*do_LOX.^2*rhoLox)./muLOX^2).^0.11)./2; %Spray Angle Calcs
```

```
    figure(1)
    plot (thetaLOX,PlLOX)
    hold on
    grid on
end
title('Pressure vs Cone Angle of LOX Injector for Different K values')
xlabel('\theta [deg]')
ylabel('Pressure [Pa]')

%% H2 Angle Approximations

d2H2 = 6.0; % Exit Diameter of H2
rH2 = (3:0.1:13.9); %[mm] From 12 to 20 mm of diameter for input of injector
rH2meter = rH2/10^3;  %conversion to meters
A0H2 = (pi*(rH2meter).^2)-A0Lox; % Area of H2 swirl chamber
rhoH2 = 0.08375; %density of H2

ApH2 = A0H2;
DsH2 = rH2meter; % diameter of changing swirl chamber
doH2 = (d2H2*2)/10^3; % diameter of exit
muH2 = 7.2057428E-6; % Dynamic viscosity of H2
KH2 = ApH2./(DsH2.*doH2); % K constant

for i=1:1:length(KH2)
    PlH2 = 1200000:1500000; % pressure range

    thetaH2 = (6*KH2(i).^-0.15.*((PlH2.*doH2.^2*rhoH2)./muH2^2).^0.11)./2; % Spray cone
calculation
```

```
    figure(2)
    plot (thetaH2,PlH2)
    hold on
    grid on
end
title('Pressure vs Cone Angle of H2 Injector for Different K values')
xlabel('\theta [deg]')
ylabel('Pressure [Pa]')
```

Appendix B – NASA CEA Results

```
        NASA-GLENN CHEMICAL EQUILIBRIUM PROGRAM CEA2, FEBRUARY 5, 2004
                    BY  BONNIE MCBRIDE AND SANFORD GORDON
     REFS: NASA RP-1311, PART I, 1994 AND NASA RP-1311, PART II, 1996

*******************************************************************************


### CEA analysis performed on Sat 06-Apr-2024 18:14:36

# Problem Type: "Rocket" (Infinite Area Combustor)

prob case=_____3211 ro

# Pressure (1 value):
p,bar= 1.7
# Chamber/Exit Pressure Ratio (1 value):
pi/p= 1.6778
# Subsonic Area Ratio (1 value):
subar= 5.1

# Oxidizer/Fuel Wt. ratio (1 value):
o/f= 5

# You selected the following fuels and oxidizers:
reac
fuel H2                wt%=100.0000  t,k= 225.000
oxid O2(L)             wt%=100.0000  t,k=  90.000

# You selected these options for output:
# short version of output
output short
# Proportions of any products will be expressed as Mass Fractions.
output massf
# Heat will be expressed as siunits
output siunits

# Input prepared by this script:/var/www/sites/cearun.grc.nasa.gov/cgi-bin/CEARU
N/prepareInputFile.cgi

### IMPORTANT:  The following line is the end of your CEA input file!
end

          THEORETICAL ROCKET PERFORMANCE ASSUMING FROZEN COMPOSITION

Pin =    24.7 PSIA
CASE = _____

            REACTANT                    WT FRACTION      ENERGY      TEMP
                                         (SEE NOTE)     KJ/KG-MOL      K
FUEL        H2                           1.0000000     -2082.407    225.000
OXIDANT     O2(L)                        1.0000000    -12979.000     90.000

O/F=    5.00000  %FUEL= 16.666667  R,EQ.RATIO= 1.587337  PHI,EQ.RATIO= 1.587337

                CHAMBER   THROAT     EXIT      EXIT
Pinf/P            1.0000   1.7857   1.6778   1.0083
P, BAR            1.7000  0.95201   1.0132   1.6859
T, K             2994.95  2697.64  2728.39  2990.51
RHO, KG/CU M    7.7443-2 4.8148-2 5.0667-2 7.6917-2
H, KJ/KG         -510.17 -1718.87 -1594.93  -528.38
U, KJ/KG        -2705.33 -3696.11 -3594.71 -2720.28
```

G, KJ/KG	-67111.1	-61708.2	-62268.2	-67030.6
S, KJ/(KG)(K)	22.2377	22.2377	22.2377	22.2377
M, (1/n)	11.344	11.344	11.344	11.344
Cp, KJ/(KG)(K)	4.1028	4.0255	4.0342	4.1018
GAMMAs	1.2175	1.2226	1.2220	1.2176
SON VEL,M/SEC	1634.8	1554.8	1563.3	1633.6
MACH NUMBER	0.000	1.000	0.942	0.117

PERFORMANCE PARAMETERS

Ae/At	1.0000	1.0031	5.1000
CSTAR, M/SEC	2270.9	2270.9	2270.9
CF	0.6847	0.6486	0.0840
Ivac, M/SEC	2826.5	2830.6	11676.6
Isp, M/SEC	1554.8	1472.9	190.8

MASS FRACTIONS

*H	0.00621	HO2	0.00001	*H2	0.06080
H2O	0.85917	*O	0.00642	*OH	0.05936
*O2	0.00803				

* THERMODYNAMIC PROPERTIES FITTED TO 20000.K

NOTE. WEIGHT FRACTION OF FUEL IN TOTAL FUELS AND OF OXIDANT IN TOTAL OXIDANTS

Appendix C – MATAKLB Calculations for Spray Cone Angle Approximation

```
clc, clear all, close all

%%

d0 = 2.4; %[mm] Lox exit diameter


rLox = 4.6; %[mm] Diameter of 2.4 to 24.2 mm for input of injector. Divided by 1000 for meters conversion

rLoxmeter = rLox/10^3;

A0Lox = pi*rLoxmeter^2;


A_LOX = pi*rLoxmeter^2;

Ds_LOX = rLoxmeter;

do_LOX = (d0*2)/10^3;


muLOX = 0.0001956;


KLOX = A_LOX/(Ds_LOX*do_LOX);


PlLOX = 250000:571200;


rhoLox = 1141; %kg/m^3

thetaLOX = (6*KLOX.^-0.15.*((PlLOX.*do_LOX.^2*rhoLox)./muLOX^2).^0.11)./2;


figure(1)

plot (thetaLOX,PlLOX)

hold on

grid on
```

```
title('Pressure vs Cone Angle of LOX Injector for Siwrl Diameter of 4.6mm')
xlabel('\theta [deg]')
ylabel('Pressure [Pa]')

%% H2 Approx

d2H2 = 6.0;
rH2 = 14; %[mm] From 12 to 20 mm of diameter for input of injector
rH2meter = rH2/10^3;
A0H2 = (pi*(rH2meter).^2)-A0Lox;
rhoH2 = 0.08375;

ApH2 = pi*rH2meter.^2;
DsH2 = rH2meter;
doH2 = (d2H2*2)/10^3;
muH2 = 7.2057428E-6;
KH2 = ApH2./(DsH2.*doH2);


   PlH2 = 1200000:1500000;

   thetaH2 = (6*KH2.^-0.15.*((PlH2.*doH2.^2*rhoH2)./muH2^2).^0.11)./2;

   figure(2)
   plot (thetaH2,PlH2)
   hold on
   grid on
```

```
title('Pressure vs Cone Angle of H2 Injector for Diameter of 14mm')
xlabel('\theta [deg]')
ylabel('Pressure [Pa]')
```

Appendix D – K Values Number for K Graphs

K Vlaues for LOX Injector	K Values for H2
0.785398163	0.659734457
0.85084801	0.66885521
0.916297857	0.677405916
0.981747704	0.685438397
1.047197551	0.692998379
1.112647398	0.700126363
1.178097245	0.706858347
1.243547092	0.71322644
1.308996939	0.719259371
1.374446786	0.72498292
1.439896633	0.730420292
1.50534648	0.735592426
1.570796327	0.740518268
1.636246174	0.745215002
1.701696021	0.749698247
1.767145868	0.753982237
1.832595715	0.758079966
1.898045562	0.762003324
1.963495408	0.765763209
2.028945255	0.769369629
2.094395102	0.772831793
2.159844949	0.776158185
2.225294796	0.779356639
2.290744643	0.782434397
2.35619449	0.785398163
2.421644337	0.788254157
2.487094184	0.79100815
2.552544031	0.793665512
2.617993878	0.796231242
2.683443725	0.798709997
2.748893572	0.801106127
2.814343419	0.803423695
2.879793266	0.805666503
2.945243113	0.807838111
3.01069296	0.809941856
3.076142807	0.81198087
3.141592654	0.813958097
3.207042501	0.815876301

3.272492347	0.817738088
3.337942194	0.81954591
3.403392041	0.821302079
3.468841888	0.82300878
3.534291735	0.824668072
3.599741582	0.826281903
3.665191429	0.827852118
3.730641276	0.829380461
3.796091123	0.830868583
3.86154097	0.832318054
3.926990817	0.833730358
3.992440664	0.835106908
4.057890511	0.836449044
4.123340358	0.837758041
4.188790205	0.839035111
4.254240052	0.840281409
4.319689899	0.841498032
4.385139746	0.842686029
4.450589593	0.843846399
4.51603944	0.844980093
4.581489286	0.846088021
4.646939133	0.847171053
4.71238898	0.848230016
4.777838827	0.849265706
4.843288674	0.850278881
4.908738521	0.851270267
4.974188368	0.85224056
5.039638215	0.853190426
5.105088062	0.854120503
5.170537909	0.855031403
5.235987756	0.855923713
5.301437603	0.856797996
5.36688745	0.857654794
5.432337297	0.858494626
5.497787144	0.859317991
5.563236991	0.860125367
5.628686838	0.860917218
5.694136685	0.861693985
5.759586532	0.862456096
5.825036379	0.863203963
5.890486225	0.86393798

5.955936072	0.864658529
6.021385919	0.865365976
6.086835766	0.866060677
6.152285613	0.866742973
6.21773546	0.867413193
6.283185307	0.868071654
6.348635154	0.868718664
6.414085001	0.869354519
6.479534848	0.869979504
6.544984695	0.870593896
6.610434542	0.871197963
6.675884389	0.871791961
6.741334236	0.872376142
6.806784083	0.872950746
6.87223393	0.873516006
6.937683777	0.87407215
7.003133624	0.874619395
7.068583471	0.875157954
7.134033318	0.875688031
7.199483164	0.876209826
7.264933011	0.876723531
7.330382858	0.877229333
7.395832705	0.877727413
7.461282552	0.878217946
7.526732399	0.878701103
7.592182246	0.879177049
7.657632093	0.879645943
7.72308194	0.880107942
7.788531787	0.880563196
7.853981634	0.881011853
7.919431481	0.881454054